Aerodynamics Department
Report Number 50

TURBULENT DIFFUSION IN THE WAKE OF A BLUNT-NOSED BODY AT HYPERSONIC SPEEDS

Prepared by

Lester Lees

Leslie Hromas

SPACE TECHNOLOGY LABORATORIES, INC.
Los Angeles 45, California

6110-0004-MU-000

Contract No. AF 04(694)-1

July 1961

SPACE TECHNOLOGY LABORATORIES, INC.
P. O. Box 95001
Los Angeles 45, California
Under Contract AF 04(694)-1

Prepared: Lester Lees

Lester Lees
Consultant, and Professor
of Aeronautics, California
Institute of Technology

Leslie Hromas

Leslie Hromas
Gas Dynamics Research Section

Approved: A. G. Hammitt

A. G. Hammitt, Head
Gas Dynamics Research Section

C. B. Cohen
Manager
Aerodynamics Department

ABSTRACT

At Reynolds numbers greater than about 5×10^4, corresponding to altitudes below about 180,000 ft., the hot "outer inviscid wake" behind the bow shock wave produced by a blunt-nosed body at hypersonic speeds is cooled mainly by turbulent diffusion and conduction. Turbulence originates in the "inner wake" formed by the coalescence of the free shear layers (or annulus) shed from the body surface when the boundary layer separates from the surface. As this turbulence spreads outward, it swallows enthalpy or momentum defect originally contained in the outer inviscid wake. If the turbulence is "locally similar", i.e., if it behaves at each station like a slice of a low speed "self-similar" wake, then the turbulent diffusivity grows from a low initial value near the body to a value corresponding to the total drag of the body at about 300 body diameters downstream. At flight velocities of the order of 9,000-10,000 ft./sec. the growth of the turbulent inner wake predicted on the basis of "locally similar" turbulence is in good agreement with shadowgraph measurements of wake widths behind spheres obtained in ballistic ranges in the region from 200 to 4,000 body diameters downstream of the body. Tentatively, one concludes that the turbulence mechanism in the wake with respect to a fixed observer is similar to the low speed case, in spite of the large mean temperature gradients.

In order to illustrate the behavior of an observable such as

electron density in a turbulent wake behind a blunt body, the two limiting cases of thermodynamic equilibrium and pure diffusion (zero electron-ion recombination rate) are calculated for $M_\infty = 22$ at altitudes of 100,000 ft. and 200,000 ft. Even for the case of thermodynamic equilibrium, the predicted turbulent radar trail length is about 200 body diameters at L-band (1300 mc/sec.) at 100,000 ft. altitude and about 150 body diameters for UHF (400 mc/sec.) at 200,000 ft. One interesting result is that the width of the plasma cylinder corresponding to the plasma frequency at L-band remains virtually constant at about 3.5 body diameters in the range $30 < x/d < 150$ at 100,000 ft. altitude. These results are sufficiently encouraging so that one can think about including the effects of finite chemical and electron - ion recombination rates in the analysis in order to give a more complete picture of the wake at hypersonic speeds.

CONTENTS

List of Figures

List of Symbols

1. Introduction

2. Model of the Hypersonic Wake

   2.1. Description of the Flow Pattern

   2.2. Characteristics of the Outer and Inner Wakes

      2.2.1. Outer Wake

      2.2.2. Inner Wake

   2.3. Relation between Equivalent Turbulent Diffusivity and Momentum Defect: Growth of Inner Wake

      2.3.1. Turbulent Diffusivity and Momentum Defect

      2.3.2. Growth of Inner Wake for "Locally Similar" Turbulence

3. Turbulent Diffusion Equations and Their Solution for Enthalpy and Mass Concentration

   3.1. Turbulent Diffusion of Enthalpy in the Inner Wake

   3.2. Turbulent Mass Diffusion in the Inner Wake

4. Distribution of Some Observables in the Wake: Comparison with Experiment

   4.1. Inviscid Enthalpy Profile for Axially-Symmetric Flow and Initial Conditions for Inner Wake

   4.2. Turbulent Diffusivity

   4.3. Growth of the Turbulent Inner Wake

   4.4. Effect of $(C_{D_f})_i$

CONTENTS (Cont'd.)

4.5. Mass Diffusion Calculations

4.6. Electron Distribution

5. Conclusions and Future Work

References

Appendix 1 - - Enthalpy Distribution in The Outer Wake

Appendix 2 - - Relation between Inviscid and Turbulent Mass Flux Quantities, $Y_{L_f}^{m+1}$ and $(\rho_f/\rho_\infty)\, Y_{T_f}^{m+1}$

Appendix 3 - - Some Remarks on Townsend's Experimental Results for Low-Speed Wakes; Relation between our K and Townsend's R_T

Appendix 4 - - Momentum Defect in the Inner Wake and Ordinary Drag: Estimate of Initial Drag Coefficient, $(C_{D_f})_i$

LIST OF FIGURES

1. Wake Behind Blunt Body at Hypersonic Speeds
2. Typical Inner Wake Velocity and Enthalpy Profiles Just Upstream and Downstream of Neck
3. Typical Velocity and Enthalpy Profiles at $\frac{x}{d} \cong 10$
4. Swallowing of Enthalpy Excess or Momentum Defect By Inner Wake
5. Outer Inviscid Enthalpy Profile ($M_\infty = 8.5$ and $p_\infty = 1$ ATM)
6. Outer Inviscid Enthalpy Profile ($M_\infty = 22$ and 100,000 ft. Altitude)
7. Growth of the Turbulent Diffusivity ($M_\infty = 8.5$ and $p_\infty = 1$ ATM)
8. Turbulent Wake Width ($M_\infty = 8.5$ and $p_\infty = 1$ ATM)
9. Comparison of Theory and Experiment for Turbulent Wake Width ($M_\infty = 8.5$ and $p_\infty = 1$ ATM)
10. Turbulent Wake Width ($M_\infty = 22$ and 100,000 ft. Altitude)
11. Comparison of Turbulent Wake Width for $M_\infty = 8\ 5$ and $M_\infty = 22$
12. Effect of Initial Turbulent Drag Coefficient on Wake Growth
13. Enthalpy Distribution Along the Axial Streamline ($M_\infty = 22$ and 100,000 ft. Altitude)
14. Turbulent Diffusion in the Wake ($M_\infty = 22$ and 100,000 ft. Altitude)
15. Electron Densities Along the Axial Streamline ($M_\infty = 22$ and 100,000 ft. Altitude)
16. Electron Densities Along the Axial Streamline ($M_\infty = 22$, 100,000 and 200,000 ft. Altitudes)
17. Radial Electron Density Distributions ($M_\infty = 22$ and 100,000 ft. Altitude)
18. Correlation of Experimental Bow Shock Shapes for a Hemisphere at $M_\infty \cong 8.5$
19. Bow Shock Shapes for a Hemisphere at $M_\infty = 22$ and 100,000 ft. Altitude

LIST OF SYMBOLS

A_m	coefficient defined in Eq. (24)
$B_1(\xi)$	enthalpy function defined in Eq. (3)
C_{D_o}	outer inviscid flow drag coefficient based on free stream quantities
C_{D_f}	turbulent inner wake drag coefficient based on free stream quantities
C'_{D_f}	drag coefficient defined in Eq. (17)
c_m	mass flux coefficient defined in Eq. (44a)
c_p	specific heat
d	body diameter
D	drag
$F\left(\frac{Y_T}{Y_{T_D}}\right)$	mass fraction function defined in Eq. (43a)
$F_1(z_f)$	drag function defined in Eq. (33)
$F_2(z_f)$	function defined in Eq. (37b)
$\mathcal{F}(z_f, H)$	integrand of Eq. (38) defined in Eq. (37a)
$g(z)$	enthalpy function defined in Eq. (2)
g_{m+1}	function defined in Eq. (A.1-9)

$G\left(\frac{Y_T}{Y_{T_f}}\right)$	enthalpy function defined in Eq. (3)
G_{m+1}	function defined in Eq. (15a)
$\mathcal{G}(z_f, H)$	integrand of Eq. (39) defined in Eq. (39a)
h	static enthalpy
H	enthalpy ratio, $\left(\frac{h_L}{h_\infty} - 1\right)_o$
k	heat conductivity
K'	diffusivity function defined in Eq. (7)
K	diffusivity constant defined in Eq. (10a)
K_i	mass fraction
l	axial distance
l_o	Townsend's wake width
L_{e_T}	turbulent Lewis number, $\frac{\epsilon_m}{\epsilon_T}$
$L(\xi)$	integrand of Eq. (47)
$\dot{m}$	mass flux
m	index, o for two-dimensional, 1 for axially-symmetric flow

LIST OF SYMBOLS (Cont'd.)

M	Mach number
n_e	electrons /cm^3
n_I	particle number density
p	pressure
q	heat transfer
r_n	body nose radius
Re	Reynolds number
R_T	Townsend's "universal" Reynolds number, $\frac{\ell_o \Delta u}{\epsilon_T}$
ρ	density
t	time
u	axial velocity component
Δu	$u_f - u(o)$
v	radial velocity component
x	axial coordinate
y	radial coordinate

LIST OF SYMBOLS (Cont'd.)

$\tilde{y}$	$\frac{y}{d}$
Y	Howarth-Dorodnitsyn coordinate
z	$\alpha_m Y_L$
β	velocity ratio, $\frac{u}{u_\infty}$; also inclination of wake streamline
γ	ratio of specific heats
δ	mass constant defined in Eq. (A.2-6); also boundary layer thickness
δ^*	displacement thickness
ϵ_T	turbulent thermal diffusivity
$\tilde{\epsilon}_T$	diffusivity function defined in Eq. (8)
ζ	Howarth coordinate ratio, $\frac{Y_T}{Y_{T_f}}$
θ	momentum thickness
κ	$\frac{k}{\rho C_p}$
ν	kinematic viscosity, $\frac{\mu}{\rho}$
ξ	axial coordinate, $\frac{x-x_i}{d}$
τ	shear stress

Subscripts

D	diffusion
f	front
i	initial; also species
L	outer inviscid
m	mass diffusivity
M	momentum diffusivity
O	along axis
T	turbulent
TR	transition
∞	free stream

1. Introduction

The wake produced by a body moving through a fluid medium is one of the oldest known fluid-mechanical phenomena. In calm water the wake of a sailing ship is observed for many miles behind the ship. Experimental studies of low speed wakes show that the momentum defect contained in the viscous portion of the wake spreads rather slowly into the rest of the fluid, even when the diffusion process is turbulent. High speed wake phenomena have also been noticed for a long time, but much less is known about them. When the familiar meteor trails are studied by radar echo techniques, trails at least 15 miles long are recorded at altitudes of the order of 100 miles. For small meteors the trail length is determined partly by the time required to consume the object, and partly by laminar diffusion and electron attachment processes in the wake.

Wakes produced by slender projectiles and blunt bodies at supersonic speeds have been observed in ballistic ranges by shadowgraph and other optical techniques, but until recently these observations did not extend very far behind the body. One of the most striking features of the flow field around a blunt-nosed object at supersonic speeds is the bow shock wave (Figure 1). When a missile or spacecraft enters the earth's atmosphere at hypersonic speeds a distinct, nearly paraboloidal shock surface[1]* is first formed in front of the body at altitudes of the order of 350,000 - 400,000 feet. The gas that traverses the "strong", nearly-normal portion of the bow shock wave is compressed and heated

---

* Superscripts denote references listed at end of paper.

irreversibly in the shock, and forms an "outer wake" behind the body (Figure 1). Even after isentropic expansion back to ambient pressure, which occurs in a distance of 50 - 100 diameters behind the body, the maximum gas temperature in this outer wake in thermodynamic equilibrium is about $4500^{\circ}K$ at satellite velocity, and about $6500^{\circ}K$ at a flight velocity of 40,000 ft./sec.[2]. Clearly the trail length defined in terms of observables such as electron density or gas radiation intensity is determined by the diffusion and recombination processes in this cylinder of hot gas left behind in the atmosphere.

Feldman[2] treated this problem under the assumption of thermodynamic equilibrium and a laminar or molecular diffusion prccess. Under these assumptions the problem downstream of the "pressure-controlled" portion ($x/d > 50$) is closely analogous to the cooling of a gas cylinder with a given initial temperature distribution. The time required to reduce the enthalpy is proportional to r_n^2/K, where $K = k/\rho c_p$ is the thermometric conductivity and r_n is the body nose radius, which characterizes the breadth of the initial enthalpy distribution. Here time is equivalent to ℓ/u_∞, where ℓ is distance behind the body, so that $\ell/r_n \sim u_\infty r_n/K$ = Re x Pr where Re is the Reynolds number and Pr the Prandtl number. Thus the predicted laminar trail length is very long even at high altitudes; for example for a nose radius of one foot at 250,000 feet altitude $\ell/r_n \cong 10^2 - 10^3$, depending on the observable of interest while at 60,000 feet altitude $\ell/r_n \sim 10^5 - 10^6$.

Feldman himself suggested[2] that the cooling process is much faster if turbulence is produced in the wake. One expects turbulence to originate in the flow region with the highest velocity gradients, and this region is undoubtedly the "inner wake" formed by the coalescence of the free shear layers (or annulus) shed from the body surface when the boundary layer leaves the surface (Figure 1). Experimental evidence[3] shows that transition to turbulent flow occurs downstream of the "neck" at fairly low Reynolds numbers, corresponding to altitudes of the order of 180,000 feet. Near the neck this turbulence is confined to a narrow region around the wake axis, but it soon spreads outward by feeding on the surrounding gas. Eventually all of the streamlines originally in the "outer wake" are engulfed by the turbulent inner wake. The main purpose of this paper is to analyze this swallowing process, which determines the rate of diffusion and cooling in the wake of a blunt-nosed body at hypersonic speeds.

In order to bring out the main ideas as simply as possible the assumption of thermodynamic equilibrium is retained in the present paper. The influence of finite recombination rates can be included later when the turbulent diffusion process is somewhat clearer.

In Section 2 the structure of the wake behind a blunt-nosed body at hypersonic speeds is described, and simplified representations of the outer and inner wakes are introduced. The boundary between these two regions is supposed to be a sharp "front", and the growth of the

to p 1-4

1-3

for 1-4

inner wake depends only on the gradient and value of the enthalpy at this front. Two limiting cases of the behavior of the turbulent diffusivity are studied: (1) "locally similar" turbulence, in which the flow at each station behaves like a "slice" of a low speed "self-similar" turbulent wake, so that the diffusivity is proportional to the local momentum defect or drag contained in the inner wake; (2) "frozen" diffusivity, in which the turbulent diffusivity depends only on the initial value of the drag coefficient for the inner wake at the "neck". Once the diffusivity is specified the turbulent diffusion equations for enthalpy and mass concentration can be integrated (Section 3). In Section 4, specific examples of the growth of the turbulent inner wake are calculated for comparison with measurements made in ballistic ranges. A typical reentry example is also computed at $M_\infty = 22$ and an altitude of 100,000 feet, in order to illustrate the behavior of the enthalpy distribution, and the behavior of the profiles of electron density in the wake in the two limiting cases of thermodynamic equilibrium and pure diffusion (zero recombination). Conclusions about the hypersonic wake obtained from this study are summarized in Section 5, which also contains some suggestions for future work.

2. Model of the Hypersonic Wake

2.1. Description of the Flow Pattern

In order to determine the correct initial conditions for the lateral spreading of the turbulent inner wake, we must examine the main aspects of wake formation behind a blunt body at hypersonic speeds. Shadowgraph observations supplemented by simple physical considerations show that the hypersonic viscous wake differs from its low speed counterpart in three important respects: (1) no evidence of large-scale vortex formation, even for laminar flow; (2) much greater "stability" of the laminar free shear layers; (3) an initial value of the momentum defect or "drag" contained in the inner wake (Figure 1) one to two orders of magnitude smaller than the total body drag.

Even on a bluff body, such as a sphere, separation occurs well aft of the 90° station, partly because of the falling pressure over the front half of the body, and partly because the supersonic shear layers can negotiate relatively high recompression pressure ratios (2-3) at the "neck" (Figure 1). The free shear layers (or annulus) shed from the separation line (or ring) on the body surface show a "rigidity" characteristic of supersonic, and especially hypersonic flows. Large-scale vortex formation just behind the body is apparently inhibited by the fact that violent streamline deflections would be accompanied by large pressure changes and shock wave formation. The separated flow tends to retain the direction established at the point of separation,

and the flow converges toward a minimum section or "neck", which contains the effective rear stagnation point.

When the boundary layer on the body surface is turbulent of course the free shear layer (or annulus) is also turbulent; however, if the boundary layer is laminar, the laminar free shear layers show a remarkable persistence at supersonic speeds. Experimental studies (and some stability considerations) indicate that the transition Reynolds number Re_{TR} for the laminar free shear layer, based on properties at the outer edge and the length of laminar "run", increases very rapidly with increasing local Mach number[4]. For an insulated body $Re_{TR} \tilde{=} 5 \times 10^4$ at $M_\infty = 0.5$, $Re_{TR} \tilde{=} 2 \times 10^5$ at $M_\infty = 2.0$, and $Re_{TR} = 2\text{-}3 \times 10^6$ at $M_\infty = 4.5$, the highest Mach number studied. Partly this effect is the result of the high average kinematic viscosity across the layer[5].* Downstream of the neck, on the other hand, the relevant Mach number based on the difference between the flow velocities on the axis and at the edge of the inner wake decreases rapidly with distance away from the neck, and the flow apparently becomes unstable. In addition, the inner wake is probably subjected to disturbances originating at the neck. Recent experiments at GALCIT indicate that the local transition Reynolds number in the inner wake behind an

---

* This fact was pointed out to us by Dr. Edward Zukoski, on the basis of his experience with hot wakes behind flame-holders.

insulated cylindrical rod transverse to the airstream at $M_\infty = 5.8$ is of the order of 5×10^4, based on local properties and the distance between the neck and the transition zone.[3] These considerations suggest that the regime in which the free shear layer is still laminar upstream of the neck, but transition to turbulent flow occurs not far downstream, is important in understanding diffusion processes in the wake behind a blunt body at hypersonic speeds.

As explained by Chapman[4] the fluid below the zero streamline originating at the separation point on the body is turned back at the neck because of the pressure rise produced by the flow deflection. This fluid enters the zone of recirculation just behind the body. The fluid along the zero streamline is brought to rest, while the fluid above the zero streamline, although slowed down, flows on to form the inner wake (Figure 1). In Chapman's limiting case the velocity along the zero streamline just upstream of the neck is about 60 per cent of the velocity at the outer edge of the free shear layer. Thus the static enthalpy at the outer edge of the viscous wake is about 35-40 per cent of the stagnation enthalpy in the inviscid flow. This is to be compared with the enthalpy along the zero streamline from the free shear layer which if brought to rest adiabatically has an enthalpy of about 60 per cent of the stagnation enthalpy in the inviscid flow, when the body surface is "cold".* Thus a hot core of fluid is generated in the inner

---

* If the body surface is insulated, the enthalpy on the zero streamline is about 95 per cent of the total enthalpy outside the viscous wake.

wake, but this core cools off with distance downstream of the neck. Typical velocity and enthalpy profiles just upstream and downstream of the neck are shown schematically in Figure 2.

The initial momentum defect or drag contained in the inner wake represents the sum of the skin-friction drag on the body and the momentum defect associated with the pressure rise at the neck. Since the density of the fluid in the inner wake just downstream of the neck is much lower than ambient and the neck width is usually less than one-half the body diameter, this initial drag is only a small fraction of the drag associated with the bow shock at hypersonic speeds. As we shall see later (Section 2.3) the turbulent eddy diffusivity ϵ_T is proportional to the drag coefficient of the inner wake. We conclude that the initial value of ϵ_T is much lower than the final value ($x/d \longrightarrow \infty$) corresponding to the total body drag. This fact has important consequences for the whole process of turbulent diffusion (Sections 2.3 and 3).

Near the neck the amount of momentum defect swallowed up by the growing inner wake is still small compared with the initial momentum defect, and the inner wake develops in the downstream direction almost as if it were enveloped by an external environment uniform in the direction normal to the wake axis. In addition to the usual spreading of the wake by "mixing", the physical boundaries of the wake expand because the static pressure is falling in the stream direction, and

the whole flow field is expanding. The proper length scale for the initial development of the inner wake is not the body diameter, but the momentum thickness θ of the inner wake, which is at least ten times smaller. Thus the velocity difference $\Delta u = \left[u_f - u\,(0)\right]$ across the inner wake decays to a small fraction of $(u_f)_{neck}$ in a downstream distance of the order of 100 θ to 200 θ, which corresponds to about 10 - 20 body diameters, at most. In fact when $\frac{u_f - u(0)}{u_f} \ll 1$ the mean inner wake flow downstream of transition to turbulence should exhibit a similarity of the form

$$\left[\frac{u_f - u}{(u_f)_{neck}}\right]\left[\frac{x - x_i}{\theta}\right]^{\frac{m+1}{m+2}} = f\left\{\frac{Y}{(x-x_i)^{\frac{1}{m+2}}\,\theta^{\frac{m+1}{m+2}}}\right\}$$

just as Townsend[6] found for the low-speed wake behind a cylindrical rod transverse to the air stream.* (Here Y is essentially the stream function, and m is a geometric index; m = 0 for a two-dimensional flow and m = 1 for axially-symmetric flow.) A typical velocity distribution at $x/d \tilde{=} 10$ is sketched in Figure 3a, and the corresponding enthalpy profile appears as a "turbulent pulse" at the base of the "inviscid" profile of the outer wake (Figure 3b).

When x/d is of the order of 10, the rate at which the inner wake is swallowing momentum defect originally contained in the outer wake can no

---

* Except possibly for a small effect caused by the negative pressure gradient along the wake axis.

longer be ignored. In the limiting case of "frozen" diffusivity the turbulent eddy diffusivity ϵ_T retains the value established by the initial drag of the inner wake at the neck. But in the opposite limiting case of "locally similar" turbulence, the local value of $\epsilon_T(x)$ depends on the local drag contained in the inner wake at that station. Thus $(d\epsilon_T/dx)$ depends on the rate of increase of momentum defect in the inner wake, which, in turn, depends on the product of the slope of the inviscid enthalpy profile, $(\partial h/\partial y)_{y=y_f}$, and the rate of spreading (dy_f/dx) of the inner wake. But (dy_f/dx) itself depends on ϵ_T. When $y_f/d \ll 1$, $(\partial h/\partial y)_{y=y_f}$ is small, and ϵ_T and y_f both increase slowly with distance downstream. Soon the turbulent front reaches the portion of the inviscid enthalpy profile where $(\partial h/\partial y)$ is appreciable, and one expects a rapid growth of ϵ_T and inner wake width. Eventually $(\partial h/\partial y)_{y=y_f}$ decreases again and the rate of growth of the inner wake slows down. Far downstream $(x/d \gg 1)$ most of the wake is turbulent; the turbulent diffusivity takes on a value corresponding to the total drag of the body, and similarity is again established.

2.2. Characteristics of the Outer and Inner Wakes

2.2.1. Outer Wake

In order to bring out the main features of the problem as simply as possible, we consider Reynolds numbers large enough so that the time scale for laminar diffusion in the outer wake is much longer than

the time required for the turbulent inner wake to swallow most of the momentum defect. The flow at any point in the outer wake is supposed to be unaffected by the inner wake until the turbulent "front" reaches it. Thus the enthalpy profile in the outer wake is completely specified by the inviscid flow field.* The present analysis is concerned with the region $x/d > 2 - 10$, where the static pressure is only about 5 times ambient pressure, at most. In this region the enthalpy along an inviscid streamline is a slowly varying function of static pressure, and we shall ignore the streamwise enthalpy gradient, but evaluate the local enthalpy correctly. This procedure amounts to a kind of local similarity approximation.[7]

As in most compressible flows the "proper distance" normal to the wake axis is not the physical distance y, but the Howarth-Dorodnitsyn variable Y defined by the relation

$$Y_L^m \, dY_L = (\rho_L/\rho_\infty) \tilde{y}^m \, d\tilde{y} \qquad (1)$$

where $\tilde{y} = y/d$, and the subscript "L" denotes "inviscid" or outer wake quantities. The inviscid enthalpy profile is represented by the two parameter relation

$$(h_L/h_\infty) - 1 = \left[(h_L/h_\infty) - 1\right]_0 g(\alpha_m Y_L) = H g(z) \qquad (2)$$

* The wake shock (Figure 1) introduces a slight modification (Appendix 1).

for $Y_L > Y_{L_f}$, where h denotes the complete static enthalpy, including the chemical enthalpy[7], $(h_L)_o$ is the value that the enthalpy would have along the zero streamline if the inviscid flow extended to the axis, $H = (\frac{h_L}{h_\infty} - 1)_o$, $z = \alpha_m Y_L$, and α_m is a scale factor. In the entire hypersonic wake $\frac{u_\infty - u}{u_\infty} << 1$ and $h - h_\infty \cong -u_\infty (u-u_\infty)$. To this approximation Y_L (Eq. (1)) represents the stream function, or mass flux between the axis and y, and the parameter α_m is determined by the momentum defect in the inviscid flow. In the region $x/d > 5 - 10$ the drag contribution made by the static pressure is negligible compared to the momentum defect, and (Appendix 1),

$$\alpha_m^{m+1} = \frac{4^{m+1}}{C_{D_o}} g_{m+1} \frac{H}{(\gamma_\infty - 1) M_\infty^2} \qquad \text{(A.1-9)}$$

Here C_{D_o} is the "inviscid" drag coefficient and

$$g_{m+1} = \int_0^\infty z^m g(z)\, dz \qquad \text{(A.1-10)}$$

When $x/d > 50 - 100$ the static pressure is virtually equal to the ambient pressure, the streamlines in the inviscid flow are all parallel to the wake axis, and the inviscid enthalpy profile described by Eq. (2) is independent of axial distance, in the limiting cases of "frozen" flow or thermodynamic equilibrium.*

---

*Evidently the methods of the present paper can be generalized to include chemical and electron-ion recombination.

2.2.2. Inner Wake

The present study is simplified by considering only the thermodynamic effect of the static pressure variation along the wake axis, but not its dynamic effect. Thus the shape of the turbulent mean enthalpy profile across the inner wake is invariant in the proper coordinates for a short distance downstream of the neck, and this same "similarity profile" should again appear far downstream. Although the profile shape in the intermediate region undoubtedly changes to some extent, the simplest assumption is that the mean enthalpy is described completely by two parameters -- the amplitude $(h_T(0) - h_f)$ and the wake width Y_{T_f}, i.e.,

$$\left(h_T/h_\infty\right) - \left(h_f/h_\infty\right) = B_1\left(\frac{x - x_i}{d}\right) G_T\left(\frac{Y_T}{Y_{T_f}}\right) \qquad * \qquad (3)$$

for

$$0 \leqq Y_T \leqq Y_{T_f} \quad .$$

Since the local environment surrounding the inner wake is characterized by the values of ρ_f, h_f, and u_d determined by the inviscid flow at $y = y_f$, the Howarth-Dorodnitsyn variable Y_T for the inner wake is logically defined as follows:

$$Y_T^m \, dY_T = \rho/\rho_f \, \tilde{y}^m \, d\tilde{y} \qquad (4)$$

---

* A more refined analysis taking the change in profile shape into account can always be carried out once the turbulent diffusion process is understood somewhat better than at present. Also, the function $G(Y_T/Y_{T_f})$ is arbitrary and for the present calculations is taken as a parabola.

(The relation between the inviscid and turbulent mass flux quantities Y_{L_f} and Y_{T_f} is discussed in Appendix 2.)

The two unknown functions $B_1\left(\frac{x - x_i}{\bar{d}}\right) = B_1(\varphi)$ and $Y_{T_f}(\varphi)$ are to be determined by satisfying the following two conditions (Section 3): (1) conservation of energy, as expressed by the energy integral equation across the inner wake; (2) energy balance along the inner wake axis, which relates the rate of cooling in the stream direction to the rate of turbulent heat conduction normal to the axis. In the absence of any acceptable theory of turbulent transport we adopt Reynolds'[8] hypothesis of similarity between the turbulent transfer of mass, momentum and energy. Reynolds' analogy states that

$$\frac{-\overline{v'u'}}{(\partial u/\partial y)} = -\frac{\overline{v'h'_{th}}}{(\partial h_{th}/\partial y)} = -\frac{\overline{v'K_i'}}{(\partial K_i/\partial y)} = \epsilon_T \qquad (5)$$

where h_{th} is the thermal enthalpy $= \int \bar{c}_p \, dT$, K_i is the mass fraction of the i^{th} species, and ϵ_T is the common turbulent "exchange coefficient". In other words the turbulent Prandtl and Lewis numbers are both equal to unity, and[7]

$$q = -\rho \epsilon_T (\partial h/\partial y) \qquad (6)$$

In his thorough experimental study of the low-speed turbulent wake behind a long cylindrical rod normal to the airstream, Townsend[6] found that a relation of the form $\tau = \rho \epsilon_T (\partial u/\partial y)$ is indeed satisfied by the mean velocity field not too close to the wake edges,

once the mean flow becomes "self-preserving", or "similar".* This fact must be regarded as an interesting coincidence for symmetrical wakes (Appendix 3). As Townsend points out, pure gradient diffusion cannot possibly describe the process of envelopment of fluid by the large-scale eddies at the outer boundaries of the wake. Nevertheless this empirical description is correct near the wake axis, and is therefore extremely useful in satisfying the energy equation on the wake axis (condition 2, above).

In Townsend's case the flow outside the wake is irrotational and the wake drag is constant. Once the influence of the initial conditions dies out the wake flow becomes "similar", and the wake is characterized by a "universal" Reynolds number $R_T = \frac{\Delta u \ell_o}{\epsilon_T}$ = constant, where Δu is the mean velocity difference across the wake and ℓ_o is a measure of the wake width, i.e., $\epsilon_T = (R_T)^{-1} \Delta u \ell_o$.** In spite of the fact that the inner wake exhibits similarity at hypersonic speeds only in the initial and final stages we make the crucial assumption that all along the wake axis

$$\epsilon_T = K' \Delta u \quad y_f \quad , \tag{7}$$

---

* In Townsend's notation $\epsilon_T \equiv \nu_T$.

** Townsend found the value $R_T = 12.5$ for the wake behind a cylindrical rod. Although data on axially-symmetric turbulent wakes are extremely scarce even at low speeds, the few measurements made by Hall[9] and Hislop lead to the provisional value $R_T \cong 14$.

where K' is a non-dimensional quantity dependent on fluid properties (see below), but not on the velocity difference or the wake width. According to Eq. (5), this assumption is equivalent to the statement that the intensity of turbulence at each station is proportional to the local value of Δu, and the scale is proportional to the local wake width (Appendix 3). In other words the effect of previous history on the development of the inner wake is ignored, so far as the turbulent diffusivity is concerned. The characteristic time required for internal adjustment of the turbulent motion is assumed to be very short compared to the time scale for the rate of change of ϵ_T in the axial direction, and ϵ_T is supposed to take on instantaneously the value appropriate to a locally similar flow. Later (Sections 2.3 and 3) we shall also consider the opposite limiting case of "slowly adjusting" turbulence, or "frozen" diffusivity, where the quantity $(\rho_f/\rho_\infty)\, Y_{T_f}^{\,m} \epsilon_T$ is determined only by the initial conditions in the inner wake.

The quantity K' could be regarded as an empirical function to be determined experimentally, but it is interesting to see whether K' can be related to Townsend's R_T for low-speed, isothermal wakes. Now it is well known that the transformation given by Eq. (4) reduces the heat conduction problem with variable density to an equivalent "incompressible" heat conduction problem. The heat conduction term in the energy equation specifies the equivalent turbulent diffusivity. By utilizing Eq. (4)

one finds that

$$\frac{1}{\tilde{y}^m}\frac{\partial}{\partial \tilde{y}}\left(\rho \epsilon_T \tilde{y}^m \frac{\partial h}{\partial \tilde{y}}\right) = \frac{\rho}{d^2 Y_T^m}\frac{\partial}{\partial Y_T}\left[\left(\frac{\rho}{\rho_f}\right)^2 \epsilon_T \frac{\tilde{y}^{2m}}{Y_T^m}\frac{\partial h}{\partial Y_T}\right]$$

On the axis this term becomes

$$\frac{\rho(0)}{d^2}\left(\frac{\partial^2 h}{\partial Y_T^2}\right)_0 \left[\left(\frac{\rho(0)}{\rho_f}\right)^2 \epsilon_T\right] \lim_{Y_T \to 0}\left[\frac{1}{Y_T^m}\frac{\partial}{\partial Y_T}\left(\frac{\tilde{y}^{2m}}{Y_T^{m-1}}\right)\right]$$

But (Eq. 4),

$$\tilde{y} \cong Y_T \left(\frac{\rho(0)}{\rho_f}\right)^{-(1/m+1)}$$

and the heat conduction term is reduced to the form

$$(m+1)\frac{\rho(0)}{d^2}\left(\frac{\partial^2 h}{\partial Y_T^2}\right)_{Y_T=0} \bar{\epsilon}_T$$

where the equivalent turbulent diffusivity is given by the relation

$$\bar{\epsilon}_T = \left(\frac{\rho(0)}{\rho_f}\right)^{2/(m+1)} \epsilon_T \qquad * \quad (8)$$

---

* Following Mager's[10] work, Ting[11] and Libby suggest a similar relation of the form $\bar{\epsilon}_T = (\rho/\rho_f)^2 \epsilon_T$ for two-dimensional turbulent wakes or jets (in our notation, where ρ_f is constant). They correctly point out that such a relation leads to a compressible eddy viscosity ϵ_T that varies across the flow. In the present study only turbulent heat conduction on the wake axis is involved, so this difficulty does not arise. Besides, the whole semi-empirical notion of the existence of ϵ_T is probably correct only near the wake axis (Appendix 3). On the wake axis Eq. (8) also agrees with their relation between $\bar{\epsilon}_T$ and ϵ_T for axially-symmetric wakes and jets.

According to Eqs. (7) and (8),

$$\widetilde{\epsilon}_T \cong K'\left(\frac{\rho(0)}{\rho_f}\right)^{2/(m+1)} \Delta u\, y_f \cong K'\left(\frac{\rho(0)}{\rho_f}\right)^{1/(m+1)} \Delta u\, Y_{T_f} \cdot d \quad (9)$$

If one makes

$$K' = K\left(\frac{\rho(0)}{\rho_f}\right)^{-1/(m+1)} \quad (10a)$$

then

$$\epsilon_T \cong K\ \Delta u\ Y_{T_f} \cdot d \quad (10b)$$

exactly as in Townsend's case[6]; therefore K is proportional to $(R_T)^{-1}$. The constant of proportionality depends only on the relationship between our Y_{T_f} and Townsend's ℓ_o (Appendix 3).

By adopting the value of K' specified by Eq. (10a), $\widetilde{\epsilon}_T$ is given more precisely by the following relation (Eqs. (7) and (8)):

$$\frac{\widetilde{\epsilon}_T}{u_\infty d} = K\left(\frac{\rho(0)}{\rho_f}\right)^{1/(m+1)}\left(\frac{\Delta u}{u_\infty}\right)\widetilde{y}_f \quad (11)$$

When $x/d > 5$ - 10 the total enthalpy is virtually a constant across the inner wake, equal to the total enthalpy of the inviscid flow. Also

$\frac{u_\infty - u}{u_\infty} \ll 1$ so that in the turbulent portion of the flow,

$$h - h_\infty \cong -\beta u_\infty (u - u_\infty) \tag{12}$$

where βu_∞ represents some average velocity, and $0.8 \leq \beta \leq 0.9$. To this approximation, Eq. (11) for $\tilde{\epsilon}_T$ becomes

$$\frac{\tilde{\epsilon}_T(\xi)}{u_\infty d} = \frac{K h_\infty}{\beta u_\infty^2} \left(\frac{\rho(0)}{\rho_f}\right)^{1/(m+1)} B_1(\xi) \tilde{y}_f(\xi) \tag{13}$$

2.3. Relation between Equivalent Turbulent Diffusivity and Momentum Defect: Growth of Inner Wake

2.3.1. Turbulent Diffusivity and Momentum Defect

Once we assume that the equivalent turbulent diffusivity is given by Eq. (10b) or Eq. (13), it is not surprising that the relation between $\tilde{\epsilon}_T$ and the local value of the momentum defect in the inner wake takes the same form as it does in an incompressible "similar" wake with constant drag. The momentum defect with respect to the local inviscid flow at the turbulent front is given by

$$D_f = 2(\pi)^m \int_0^{y_f} \rho u (u_f - u) y^m \, dy \qquad * \tag{14}$$

---

* The relation between this momentum defect and the ordinary drag is discussed briefly in Appendix 4.

By utilizing Eqs. (3), (4), and (12), one finds that

$$D_f = 2(\pi)^m \rho_f h_\infty d^{m+1} B_1(\varphi) Y_{T_f}^{m+1} G_{m+1} \tag{15}$$

where

$$G_{m+1} = \int_0^1 G(\varphi) \varphi^m d\varphi \tag{15a}$$

and

$$\varphi = Y_T / Y_{T_f}$$

with $G(\varphi)$ arbitrary (for the present calculations in Sections 2 and 4 a parabola is chosen). By combining Eqs. (13) and (15) we find that

$$\frac{\tilde{\epsilon}_T}{u_\infty d} Y_{T_f}^m = \frac{K\beta}{4^{m+1} G_{m+1}} \left(\frac{\rho(0)}{\rho_f}\right)^{1/(m+1)} \left(\tilde{y}_f / Y_{T_f}\right) C_{D_f}' \tag{16}$$

Here C_{D_f}' is the "local" drag coefficient defined by the relation

$$D_f = C_{D_f}' \left[\frac{(\pi)^m}{4^m} d^{m+1} \frac{\rho_f u_f^2}{2}\right] \tag{17}$$

i.e.,

$$C_{D_f}' = \left(\rho_\infty / \rho_f\right)\left(C_{D_f} / \beta^2\right) \tag{17a}$$

where C_{D_f} is the drag coefficient based on $\frac{\rho_\infty u_\infty^2}{2}$. By Eq. (4) $\tilde{y} \cong Y_T \left(\frac{\rho(0)}{\rho_f}\right)^{-1/(m+1)}$, so that

$$\frac{\tilde{\epsilon}_T}{\beta u_\infty d} Y_{T_f}^{m} \cong \frac{K}{4^{m+1} G_{m+1}} C_{D_f}' \qquad * \quad (18)$$

or,

$$\frac{\rho_f}{\rho_\infty} \left(\frac{\tilde{\epsilon}_T}{u_\infty d}\right) Y_{T_f}^{m} \cong \frac{K/\beta}{4^{m+1} G_{m+1}} C_{D_f} \qquad (18a)$$

For "locally similar" turbulence C_{D_f} in Eq. (18a) is the local value of the drag coefficient. Thus the quantity

$$\frac{\rho_f}{\rho_\infty} \left(\frac{\tilde{\epsilon}_T}{u_\infty d}\right) Y_{T_f}^{m}$$

increases from its initial value corresponding to $(C_{D_f})_i$ to the final value far downstream corresponding to the total drag coefficient of the body. The opposite limiting case of "slowly-adjusting" turbulence is characterized by "freezing" the quantity $(\rho_f/\rho_\infty)\left(\frac{\tilde{\epsilon}_T}{u_\infty d}\right) Y_{T_f}^{m}$ at its initial value corresponding to $(C_{D_f})_i$.

A precise value of $(C_{D_f})_i$ is difficult to determine a priori, but a rough estimate is obtained by equating $(D_f)_i$ to the sum of the skin friction drag of the body and the additional momentum defect produced by the pressure rise associated with the flow deflection at the neck. The analysis in Appendix 4 indicates that $(C_{D_f})_i$ varies with Reynolds number like $Re^{-\frac{1}{2}}$ when the free shear layer is laminar. According to Eq. (A. 4-9) at $Re_d = 10^5$, $(C_{D_f})_i \cong 0.02$ for axially-symmetric flow, so that $(C'_{D_f})_i \cong 0.04$ at $M_\infty = 6$, while $(C'_{D_f})_i \cong 0.2$ at $M_\infty = 20$.

---

* The "exact" expression for ϵ_T (Eq. (13) or (16)) is utilized in the detailed computations of Sections 3 and 4.

The actual estimated value of $(C_{D_f}')_i$ is less significant than the fact that it is at least one order of magnitude lower than the total body drag coeffcient for a bluff body at hypersonic speeds. According to Eq. (18) the initial value of $\frac{\widetilde{\epsilon}_T}{u_\infty d} Y_{T_f}^m$ (or the "frozen" value for "slow" turbulence) is also one order of magnitude lower than the value corresponding to turbulent flow across the major portion of the outer wake.

By employing Eqs. (15) and (17) we have

$$\frac{B_1(\varphi)}{H} Y_{T_f}^{m+1} = \frac{(\gamma_\infty - 1) M_\infty^2}{H} \frac{\beta^2 C_{D_f}'}{4^{m+1} G_{m+1}} \tag{19}$$

Thus, once $(C_{D_f}')_i$ is known the initial value of Y_{T_f} is determined by the value of B_1/H selected to start the computations. In other words, B_1/H, $(C_{D_f})_i$, and H are the parameters of the problem. If $(Y_{T_f})_i \ll 1$ one expects the subsequent development of the wake to be relatively insensitive to the particular value of $(Y_{T_f})_i$ selected (Section 4).

2.3.2. Growth of Inner Wake for "Locally-Similar" Turbulence

Although small, the initial value of $\frac{\widetilde{\epsilon}_T}{u_\infty d}$ plays an important role in determining the initial rate of growth of the inner wake once the pressure approaches ambient. For "locally similar" turbulence this initial growth rate determines the location downstream of the body at which the inner wake begins to swallow appreciable momentum defect from the outer wake, and thereby to increase $\frac{\widetilde{\epsilon}_T}{u_\infty d}$ in accordance with

with Eq. (18). In Figure 4, the momentum defect contained in the inner wake is represented by the arca under the curve of enthalpy ratio

$$\frac{h_T - h_f}{h_\infty} \quad \text{vs.} \quad Y_T$$

(Eqs. (12), (14), and (15)). From this figure one sees that

$$\frac{dD_f}{d\xi} = -2(\pi)^m \rho_f h_\infty \frac{Y_{T_f}^{m+1}}{m+1} d^{m+1} \frac{d}{d\xi}\left(\frac{h_f}{h_\infty}\right) \quad * \quad (20)$$

where the right-hand side represents the swallowing rate. By employing Eqs. (17) and (20) we find that

$$\beta^2 \frac{d}{d\xi}\left(\frac{\rho_f}{\rho_\infty} C_{D_f}'\right) = -4^{m+1}\left(\frac{h_\infty}{u_\infty}\right)\frac{\rho_f}{\rho_\infty} \cdot \frac{Y_{T_f}^{m+1}}{m+1}\left[\frac{d}{dY_L}\left(\frac{h_L}{h_\infty}\right)\right]_{Y_L=Y_{L_f}} \frac{dY_{L_f}}{d\xi} \quad (21)$$

and by using Eqs. (2) and (18) we have

$$\frac{d}{d\xi}\left(\frac{\rho_f}{\rho_\infty}\frac{\bar{\epsilon}_T}{u_\infty d} Y_{T_f}^m\right) = -\frac{K\alpha_m}{\beta(m+1)G_{m+1}} \frac{H}{(\gamma_\infty - 1)M_\infty^2} \frac{\rho_f}{\rho_\infty} Y_{T_f}^{m+1} g'(Z_f) \frac{dY_{L_f}}{d\xi} \quad (22)$$

But the energy balance along the wake axis (Section 3) leads to a relation of the form

$$N_1(Y_{L_f}) \frac{dY_{L_f}}{d\xi} = \left(\frac{\bar{\epsilon}_T}{u_\infty d}\right)$$

which together with Eq. (22), yields a differential equation for $\frac{\bar{\epsilon}_T}{u_\infty d} Y_{T_f}^m$ of the form

$$\frac{d}{d\xi}\left(\frac{\rho_f}{\rho_\infty}\frac{\bar{\epsilon}_T}{u_\infty d} Y_{T_f}^m\right) = -\left[N_2(Y_{L_f}) g'(Z_f)\right]\left(\frac{\bar{\epsilon}_T}{u_\infty d} Y_{T_f}^m \frac{\rho_f}{\rho_\infty}\right)$$

---

* A proof of this relation is given in Section 3.1.

This last relation clearly shows the exponential character of the growth of the turbulent diffusivity, but the amplification factor depends strongly on the slope of the inviscid enthalpy profile $g'(z_f)$, as expected (Section 4).

In the initial stages $z_f \ll 1$ and $g'(z_f) \ll 1$, so that the rate of growth of the inner wake is given by an expression closely resembling the usual similarity relation (Section 3):

$$Y_{T_f}^{m+1} \frac{dY_{T_f}}{d\xi} = -\frac{K}{4^{m+1}} \frac{G''(0)}{G_{m+1}} \left(C_{D_f}'\right)_i^{\frac{1}{2}} \quad . \quad (23)$$

By taking $g'(z_f) = -2z_f$ (Appendix 1), and by using Eq. (23) and the approximate relation $(\rho_f/\rho_\infty)\, Y_T^{m+1} = Y_L^{m+1}$ (Appendix 2), the differential equation Eq. (22) for $\frac{\tilde{\epsilon}_T}{u_\infty d}$ can be integrated, and the result is as follows, for $z_f \ll 1$:

$$\frac{\tilde{\epsilon}_T}{u_\infty d} Y_{T_f}^{m} = \left(\frac{\tilde{\epsilon}_T}{u_\infty d} Y_{T_f}^{m}\right)_i \left[1 + A_m \xi^{\frac{m+3}{m+2}} + \ldots\right] \quad (24)$$

where

$$A_m = \frac{1}{2^{m/(m+2)}} \left(-\frac{KG''(0)}{\beta^2 G_{m+1}} m+2\right)^{\frac{m+3}{m+2}} \left(\frac{\alpha^2 m}{m+1}\right) \left(\frac{1}{m+3}\right) \left(\frac{H}{(\gamma_\infty - 1) M_\infty^2}\right) \left(C_{D_f}\right)_i^{\frac{1}{m+2}} \left(\frac{\bar{\rho}_f}{\rho_\infty}\right)^{\frac{(m+3)}{(m+1)(m+2)}}$$

and $(\bar{\rho}_f/\rho_\infty)$ denotes a suitable average value of (ρ_f/ρ_∞). If the

turbulent mean enthalpy profile is chosen to be a parabola then

$$G_1 = 2/3, \quad G_2 = 1/4, \quad G''(0) = -2 \quad .$$

Also,

$$\frac{H}{(\gamma_\infty - 1) M_\infty^2} \cong \frac{1}{6}$$

over a wide range of Mach numbers for equilibrium conditions (Appendix 1). As an illustration we take $g(z) = e^{-z^2}$, so that (Eq. (A.1-10)), $g_1 = \sqrt{\pi/2}$ and $g_2 = \frac{1}{2}$; then

$\alpha_o^2 \cong 0.36$ and $\alpha_1^2 \cong 1.35$ for $C_{D_o} = 1$ (Eq. (A.1-9)).

With K = 0.04 (Appendix 3) and $\beta = 0.9$ one obtains

$$A_o \cong 0.0033 \, (\overline{\rho_f}/\rho_\infty)^{3/2} \, (C_{D_f})_i^{\frac{1}{2}} \qquad (25)$$

$$A_1 \cong 0.03 \, (\overline{\rho_f}/\rho_\infty)^{2/3} \, (C_{D_f})_i^{1/3}$$

Fortunately the axial distance required to increase the effective turbulent diffusivity by a specified factor is relatively insensitive to the value of $(C_{D_f})_i$. This distance varies like $(C_{D_f})_i^{-1/3}$ in the two-dimensional case, and like $(C_{D_f})_i^{-1/4}$ in the axially-symmetric case. However, this distance varies directly with $(\overline{\rho_f}/\rho_\infty)^{-1}$ for two-dimensional flow, and like $(\overline{\rho_f}/\rho_\infty)^{-\frac{1}{2}}$ for axially-symmetric flow.

At $Re_d = 10^5$, $(C_{D_f})_i = 0.014$ in the two-dimensional case and $(C_{D_f})_i = 0.02$ for axially-symmetric flow (Appendix 4).

At $M_\infty = 6$, $(\overline{\rho_f}/\rho_\infty) \cong 0.39$. According to Eqs. (24) and (25), the

distance required to increase the initial diffusivity $(\widetilde{\epsilon}_T / u_\infty d)\, Y_{T_f}{}^m$ by 50 per cent is about 300 diameters in the two-dimensional case and about 35 diameters in the axially-symmetric case. At $M_\infty = 20$, $(\overline{\rho}_f/\rho_\infty) \cong 0.033$. Here the corresponding axial distance is about 3500 diameters (!)* for two-dimensional flow and about 120 diameters for axially-symmetric flow. The marked difference between two-dimensional and axially-symmetric flow is caused by two related factors: (i) the hot gas in the inviscid flow is concentrated much closer to the wake axis in the axially-symmetric case; (ii) the axially-symmetric inner wake swallows mass (and momentum defect) much more rapidly than its two-dimensional counterpart, again because of the geometric factor. The growth of $\widetilde{\epsilon}_T/u_\infty d$ for the axially-symmetric inner wake is indicated schematically in the accompanying sketch.

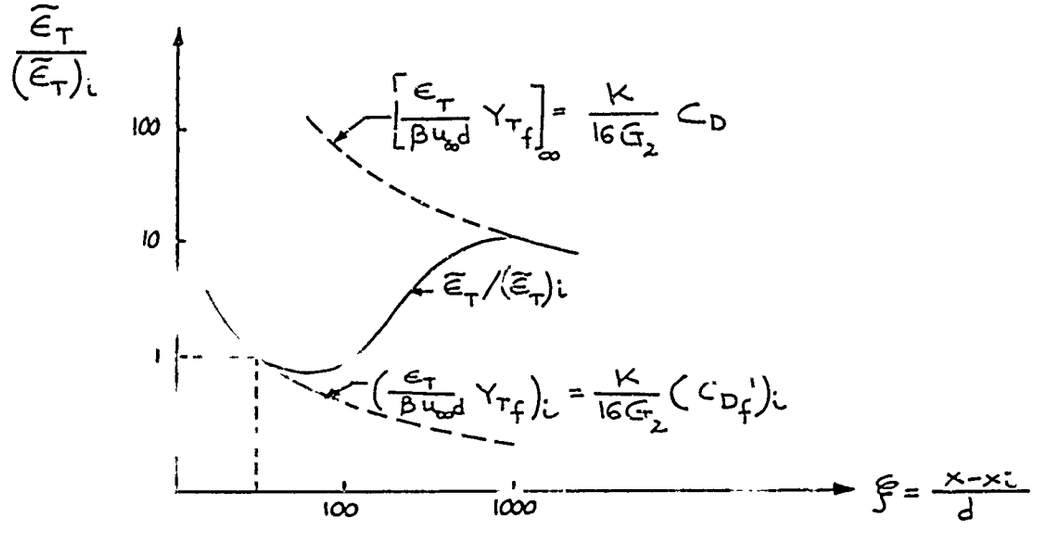

* In other words this distance is so large that the quantity $(\rho_f/\rho_\infty)\,(\widetilde{\epsilon}_T/u_\infty d)$ is virtually constant at its initial value.

3. Turbulent Diffusion Equations and Their Solution for Enthalpy and Mass Concentration

3.1. Turbulent Diffusion of Enthalpy in the Inner Wake

In a steady, two-dimensional or axially-symmetric turbulent flow of boundary layer type the energy equation for the complete static enthalpy of an effective binary mixture takes the following form[7]:

$$\rho\left(u\frac{\partial h}{\partial x}+v\frac{\partial h}{\partial y}\right)=\frac{1}{y^m}\frac{\partial}{\partial y}\left(\rho\epsilon_T y^m\frac{\partial h}{\partial y}\right)+\rho\epsilon_M\left(\frac{\partial u}{\partial y}\right)^2 + u\frac{\partial p}{\partial x}+\frac{1}{y^m}\frac{\partial}{\partial y}\left[\rho\epsilon_m\left(1-\frac{1}{Le_T}\right)y^m\sum h_i\frac{\partial K_i}{\partial y}\right] \tag{26}$$

Here ϵ_T, ϵ_M, and ϵ_m are the turbulent thermal, momentum, and mass diffusivities, respectively, and Le_T is the turbulent Lewis number = (ϵ_m/ϵ_T). The laminar contribution to the transport and dissipation terms is regarded as negligible in comparison to the main turbulent contributions.

The relative importance of the dissipation term in the wake is measured by the ratio

$$\frac{(\Delta u)^2}{\left[\left(\frac{h_L}{h_\infty}\right)_o-1\right]}$$

where $\Delta u = u_f - u\,(0)$. In hypersonic wakes this term is negligible. The statement that $Le_T = 1$ eliminates the last term in Eq. (26). (This statement is not necessary in formulating the energy integral equation. (See below.)) As explained in Section 2 only the thermodynamic effect of the static pressure variation, but not its dynamic

effect, is taken into account here. With these approximations Eq. (26) becomes

$$\rho\left(u\frac{\partial h}{\partial x}+v\frac{\partial h}{\partial y}\right)=\frac{1}{y^m}\frac{\partial}{\partial y}\left(\rho\epsilon_T y^m\frac{\partial h}{\partial y}\right) \tag{27}$$

By the usual order of magnitude considerations for wake flows[12] $v(\partial h/\partial y) \ll u(\partial h/\partial x)$ not too close to the neck. Also $u \cong \bar{u} = \beta u_\infty$, where $0.80 \leq \beta \leq 0.90$. Thus the present problem is analogous to a problem in one-dimensional (m= 0) or cylindrical (m = 1) non-steady heat conduction, with $t = x/\bar{u}$. However, the situation is somewhat unusual, because ϵ_T itself depends on the amplitude and breadth of the enthalpy pulse (Eqs. (8) and (13)), and "heat" is spreading into a region ($y > y_f$) containing a time-independent non-uniform enthalpy distribution, but in which ϵ_T is effectively zero. The diffusion of a material property is governed by an equation similar to Eq. (27) (Section 3.2).

By introducing the Howarth-Dorodnitsyn variable (Eq. (4)), and by making use of the continuity equation, Eq. (27) is converted to the form

$$u\frac{\partial h}{\partial \xi}+\tilde{v}\frac{\partial h}{\partial Y_T}=\frac{1}{Y_T^m}\frac{\partial}{\partial Y_T}\left[\left(\frac{\rho}{\rho_f}\right)^2\frac{\epsilon_T}{d}\frac{\tilde{y}^{2m}}{Y_T^m}\frac{\partial h}{\partial Y_T}\right] \tag{28}$$

where $\xi = x/d$, $\tilde{y} = y/d$, and $\tilde{v}$ is the lateral velocity in the "equivalent incompressible flow" given by the relation $\tilde{v} = u\,Y_\xi + v\,Y_y$. As shown

in Section 2 the effective thermal diffusivity $\widetilde{\epsilon}_T$ is defined by

$$\left(\frac{\rho}{\rho_f}\right)^2 \left(\frac{\tilde{y}}{Y_T}\right)^{2m} \frac{\epsilon_T}{u_\infty d} \simeq \left(\frac{\rho(0)}{\rho_f}\right)^{2/(m+1)} \frac{\epsilon_T}{u_\infty d} = \frac{\widetilde{\epsilon}_T}{u_\infty d} \qquad *$$

Instead of seeking "exact" analytic solutions to Eqs. (27) or (28) we integrate Eq. (27) across the inner wake, thereby converting it into a first-order, non-linear ordinary differential equation for the enthalpy excess, or momentum defect contained in the inner wake. A second equation of this type is supplied by satisfying Eq. (27) all along the wake axis.** These two equations are sufficient to determine the behavior of the two parameters $B_1(\xi)$ and $Y_{T_f}(\xi)$ (Eq. (3)), and thus all characteristics of the turbulent diffusion of enthalpy.

---

* Actually the transformation to an "equivalent incompressible flow" is strictly valid only along the wake axis, because ρ_f is not constant.

** Additional integrals, or higher "moments" of Eq. (27) can be employed later if greater accuracy is found to be necessary.

By multiplying Eq. (27) by y^m, integrating across the inner wake, and utilizing the continuity equation and Eq. (4), one obtains

$$\frac{d}{d\xi}\left[\int_0^{Y_{T_f}} \rho_f u_T h Y_T^m \, dY_T\right] = h_f \frac{d}{d\xi}\left[\int_0^{Y_{T_f}} \rho_f u_T Y_T^m \, dY_T\right] \qquad * \text{ (29)}$$

or

$$\frac{d}{d\xi}\left[\int_0^{Y_{T_f}} \rho_f (h-h_f) Y_T^m \, dY_T\right] = -\rho_f \frac{Y_{T_f}^{m+1}}{m+1} \frac{dh_f}{d\xi} \qquad (30)$$

where u has been replaced by $\bar{u}$, and thereby eliminated from Eq. (30). The integral on the left-hand side of Eq. (30) is proportional to

---

* The heat transfer rate $\dot{q}(y_f)$ at the interface between the inner and outer wakes ($y = y_f$) is supposed to be negligible compared to the rate at which enthalpy is entrained at this interface. Since

$$\dot{q}(y_f) = \dot{q}_L(y_f) = \frac{-k_L}{c_{p_L}} \left(\frac{\partial h_L}{\partial y}\right)_{y=y_f}$$

this approximation is correct if

$$-\frac{k_L}{c_{p_L}} (\partial h/\partial y)_L \Big/ h_f \frac{d\dot{m}}{dx} \ll 1$$

or if

$$\frac{u_\infty d}{\nu_f} \frac{dy_f}{dx} \gg 1$$

the momentum defect (Eqs. (12) and (14)). By introducing Eq. (3) for the turbulent enthalpy profile, and employing Eq. (2), one has

$$\frac{d}{d\xi}\left[\frac{\rho_f}{\rho_\infty} B_1(\xi)(Y_{T_f})^{m+1} G_{m+1}\right] = -\left(\frac{\rho_f}{\rho_\infty}\right)\frac{\alpha_m (Y_{T_f})^{m+1}}{m+1}\left[\left(\frac{h_L}{h_\infty}\right)_o - 1\right] g'(\alpha_m Y_{L_f})\frac{dY_{L_f}}{d\xi} \qquad (31)$$

This last equation is identical to the relation obtained from Figure 4 by intuitive considerations (Eq. (20); now the basic assumptions underlying this relation are clear. Integration of Eq. (31) yields

$$\frac{\rho_f}{\rho_\infty} B_1(\xi) Y_{T_f}^{m+1} G_{m+1} = \left[\frac{\rho_f}{\rho_\infty} B_1(\xi) Y_{T_f}^{m+1} G_{m+1}\right]_i - \frac{\left[\left(\frac{h_L}{h_\infty}\right)_o - 1\right]\alpha_m}{m+1}\int_{(Y_{L_f})_i}^{Y_{L_f}} \frac{\rho_f}{\rho_\infty} Y_{T_f}^{m+1} g'(\alpha_m Y_{L_f})\, dY_{L_f} \qquad (32)$$

By recognizing that (Appendix 2)

$$(\rho_f/\rho_\infty) Y_{T_f}^{m+1} = Y_{L_f}^{m+1} - \delta(\text{constant}), \ * \qquad (A.2\text{-}6)$$

---

* For $(\xi - \xi_i) > 100$, $\delta << Y_{L_f}^{m+1}$

and employing Eq. (A. 1-9) for α_m^{m+1}, Eq. (32) is rewritten in a convenient form defining a "drag function" $F_1(z_f)$:

$$\frac{\frac{\rho_i}{\rho_\infty} B_1 Y_{T_f}^{m+1} \bar{G}_{m+1}}{\left(\frac{\rho_f}{\rho_\infty} B_1 Y_{T_f}^{m+1} G_{m+1}\right)_i} = \frac{C_{Df}}{(C_{Df})_i} = F_1(z_f) = 1 + \frac{H}{H+1}\left[g(z_f) - g(z_{f_i})\right] \tag{33}$$

$$+ \frac{C_{Do}}{(C_{Df})_i} \frac{1}{g_{m+1}} \left\{ \int_{z_{f_i}}^{z_f} z^m g(z)\, dz - \left[\frac{z^{m+1} g(z_f)}{m+1} \right]_{z_{f_i}}^{z_f} \right\}$$

where $z_f = \alpha_m Y_{L_f}$ and $H = (h_L/h_{\infty})_o - 1$.

Along the wake axis Eq. (27) or (28) becomes

$$\left(\frac{\partial h}{\partial \xi}\right)_{Y_T=0} = (m+1)\left(\frac{\partial^2 h}{\partial Y_T^2}\right)_{Y_T=0} \left(\frac{\bar{\varepsilon}_T}{\beta u_\infty d}\right) \tag{34}$$

By using Eq. (3) for the turbulent enthalpy profile, one obtains

$$H g(z_f) \frac{dz_f}{d\xi} + \frac{dB_1}{d\xi} = (m+1) \frac{G''(0)}{Y_{T_f}^2} B_1 \left(\frac{\bar{\varepsilon}_T}{\beta u_\infty d}\right) \tag{35}$$

For "locally similar" turbulence $\bar{\varepsilon}_T$ is given by Eq. (16). By utilizing Eqs. (17a), (33), and (A.2-6), one finds that

$$\frac{\widetilde{\epsilon}_T}{\beta u_\infty d} = \frac{\alpha_m^m K(C_{Df})_i}{\beta^2 4^{m+1} G_{m+1}} \left(\frac{\rho(0)}{\rho_f}\right)^{1/(m+1)} \left(\frac{\alpha_m \tilde{v}_f}{z_f}\right) \frac{z_f F_1(z_f)}{\left(z_f^{m+1} - \alpha_m^{m+1} \delta\right)} \quad (36)$$

Now $(dB_1/d\xi)$ can be eliminated in favor of $(dz_f/d\xi)$ by employing Eqs. (31) and (A.2-6), and B_1 itself is expressed in terms of z_f by using Eq. (33). For simplicity we take $\rho \sim (p/h)$. Finally one has

$$\mathcal{F}(z_f, H)(dz_f/d\xi) = -(K/\beta^2) \frac{G''(0)}{4^{m+1} G_{m+1}} \alpha_m^{m+2} (C_{D_f})_i (p_f/p_\infty)^{1/(m+1)} \quad (37)$$

where

$$\mathcal{F}(z_f, H) = \frac{z_f^{m-1}\left(z_f^{m+1} - \alpha_m^{m+1}\delta\right)^{2/(m+1)} \left(\frac{h(0)}{h_\infty}\right)^{\frac{1}{m+1}} \left(\frac{h_f}{h_\infty}\right)^{\frac{1}{m+1}}}{\left[\left(\frac{p_f}{p_\infty}\right)^{1/m+1} \quad \frac{\alpha_m \tilde{v}_f}{z_f}\right]} \cdot \frac{F_2(z_f)}{F_1(z_f)} \quad (37a)$$

and

$$F_2(z_f) = \left[1 + \frac{1}{m+1}\left\{\frac{1}{(m+1)G_{m+1}} - 1\right\} \frac{G_{m+1}}{g_{m+1}} \frac{C_{Do}}{(C_{Df})_i} g'(z_f) \frac{\left(z_f^{m+1} - \alpha_m^{m+1}\delta\right)^2}{z_f^m F_1(z_f)}\right] \quad (37b)$$

$F_1(z_f)$ is defined by Eq. (33),

$$\alpha_m^{m+1}\delta = (m+1) g_{m+1} \frac{H}{H+1} \frac{C_{Df_i}}{C_{D_o}} \quad (A.2\text{-}8)$$

$$\frac{h(0)}{h_\infty} = 1 + H\left[\mathcal{J}(z_1) + \frac{B_1}{H}\right] \tag{37c}$$

with (Eq. (33)),

$$\frac{P}{\quad} \quad \frac{(\quad)_i}{C_{D_0}} \quad \frac{\mathcal{J}_{m+1}}{G_{m+1}} \quad \frac{F_1(z_f)}{(\quad)} \tag{37d}$$

Also

$$\left(\frac{P_f}{P_\infty}\right)^{1/(m+1)} \left(\frac{\quad}{z_T}\right) = \left[1 + \frac{(m+1)H}{\quad} \int_0^{z_f} \mathcal{J}(\xi)\, d\xi\right]^{1/(m+1)} \tag{37e}$$

and

$$\frac{h_f}{\quad} = -Hg(z_f) \tag{37f}$$

The function $\mathcal{J}(z_f, H)$ in Eq. (37) depends on ξ only through the slow variation of H with decreasing (p_f/p_∞) along the wake axis. Therefore, $\mathcal{J}(z_f, H)$ is practically a function of z_f alone, and Eq. (37) can be converted into a single quadrature for the growth of the turbulent inner wake:

$$\int_{z_{T_i}}^{z_f} \mathcal{J}(z_f, H)\, dz_f = -\frac{K}{\beta^2} \frac{G'(0)}{4^{m+1} G_{m+1}} (\quad)_i \left(\frac{P_\perp}{P_\infty}\right)^{\quad} \quad (38)$$

The static pressure distribution along the wake axis must be obtained from a theoretical solution for the inviscid flow including the wake shock (Figure 1), or from experiments. Of course for $\xi > 100$, $(p_f/p_\infty) \doteq 1$. Once $z_f(\xi)$ is known from Eq. (38) the physical wake boundary is determined from Eq. (37e), and the amplitude of the turbulent pulse is given by Eq. (37d).

In the opposite limiting case of "frozen" diffusivity from Eq. (18a)

$$\frac{\rho_f}{\rho_\infty}\frac{\bar{\epsilon}_T}{\beta u_\infty d} Y_{T_f}^{\,m} \cong \frac{K}{\beta^2 4^{m+1} G_{m+1}} (C_{D_f})_i \qquad (18a)^*$$

and by using Eqs. (31), (33), and (A.2-6) the heat conduction equation (Eq. (35)) is converted to the following single quadrature:

$$\int_{z_{f_i}}^{z_f} \mathcal{G}(z_f, H)\, dz_f = \frac{-K}{\beta^2}\frac{G''(0)}{4^{m+1} G_{m+1}} \alpha_m^{\,m+2} (C_{D_f})_i \int_{\xi_i}^{\xi} \left(\frac{p_f}{p_\infty}\right)^{1/(m+1)} d\xi \qquad (39)$$

where

$$\mathcal{G}(z_f, H) = z_f^{\,m}\left(z_f^{\,m+1} - \alpha_m^{\,m+1}\xi\right)^{1/(m+1)} \left(\frac{h_f}{h_\infty}\right)^{1/(m+1)} F_2(\bar{z}_f) \qquad (39a)$$

---

* The exact value of the initial diffusivity given by Eq. (16) or Eq. (36) is used in the calculations discussed in Section 4.

with $F_2(z_f)$ defined by Eq. (37b), and (h_f/h_∞) given by Eq. (37f).

In the region not too close to the neck, but before appreciable "swallowing" has begun,

$$\alpha_m^{m+1} \delta << z_f^{m+1} << 1 \;,\; F_1(z_f) \cong 1 \;,\; F_2(z_f) \cong 1 \;,$$

$$\frac{h(0)}{h_\infty} \cong 1 + H, \left(\frac{\alpha_m \tilde{y}_f}{z_f}\right)\left(\frac{p_f}{p_\infty}\right)^{1/(m+1)} \cong (1+H)^{1/(m+1)}$$

Thus the solution of both Eqs. (37) and (39) is reduced to the similarity relation

$$Y_{T_f}^{m+2} - (Y_{T_f})_i^{m+2} = -(m+2)\frac{K}{\beta^2}\frac{G''(0)}{4^{m+1}G_{m+1}}(C_{D_f})_i(\xi - \xi_i) \quad (40)$$

However, the outward growth of the physical boundary of the inner wake is strongly influenced by the falling static pressure along the wake axis in this region (Eqs. (A.2-6) and (37e)).

Once the swallowing process begins, the solutions for "locally similar" turbulence and "frozen" diffusivity diverge, of course, and it is difficult to give any precise estimates of the wake growth. For locally similar, axially-symmetric turbulent wakes, however, the swallowing process is virtually completed 100-200 body diameters down-

stream of the neck, so that $F_1(z_f) \cong \frac{C_{D_o} + (C_{D_f})_i}{(C_{D_f})_i}$ and $F_2(z_f) = 1$ for $\xi - \xi_i > 100 - 200$. Roughly speaking (Eqs. (37), (37a), (37c) - (37f))

$$\tilde{z}_+ \sim \left[K(C_{D_o} + C_{D_{f_i}})\right]^{(\quad)} (H)^{-\frac{\quad}{(m+1)(m+2)}} \xi^{(\quad)} \qquad (41)$$

and

$$\tilde{y}_f \sim \tilde{z}_+ H^{(\quad)} \sim \left[K(C_{D_o} + C_{D_{f_i}}) H^{m(\quad)} \xi\right]^{1/(m+2)} \qquad (42)$$

Thus the wake width at a given ξ is not very sensitive to H (or flight velocity). The growth of the wake is given more accurately by Eq. (37e); this relation takes into account the cooling effect, which makes the wake grow more slowly than an isothermal wake. Numerical calculations are required to illustrate the actual behavior of the wake. (Section 4).

Far downstream ($\xi > 10^4$) the wake has cooled off sufficiently so that $\frac{h(0)}{h_\infty} \cong 1$, $\frac{h_f}{h_\infty} \cong 1$, and $\frac{\alpha_m \tilde{y}_f}{z_f} \cong 1$. In this regime the growth of the wake is described by a relation like Eq. (40), with $C_{D_{f_i}}$ replaced by $(C_{D_o} + C_{D_{f_i}})$ for "locally similar" turbulence. The enthalpy distribution takes on the self-similar behavior analogous to Townsend's case:

$$G(\quad)\left[\frac{h_\tau - h_f}{\left(\frac{h_\infty}{2}\right)}\right]\left(\frac{Ax}{\theta}\right)^{\frac{\quad}{m+2}} = G\left[\frac{y}{(2Ax)^{(\quad)}\theta^{\frac{m+1}{m+2}}}\right]$$

where

$$A = -(m+2)\frac{K}{\beta^2}\,\frac{G''(0)}{4^{m+1}G_{m+1}}$$

and θ is the momentum thickness defined by

$$\left(\frac{\theta}{d}\right)^{m+1} = \frac{C_{D_0} + C_{D_{f_i}}}{2^{2+m}}$$

3.2. Turbulent Mass Diffusion in the Inner Wake

Once the history of the turbulent diffusivity $\epsilon_T(\xi)$ along the wake axis is known, turbulent diffusion of a particular chemical species in the inner wake can also be described by an analysis similar to that employed for the complete static enthalpy (Section 3.1). As an illustrative example, consider the simplest case in which all of the diffusing species is confined within the inner wake, and recombination or other chemical reactions involving this species are so much slower than diffusion that they can be ignored. Such a situation might arise when an ablating body deposits a "foreign" substance into the boundary layer.

In analogy to Eq. (3) for the enthalpy, the simplest representation of the mass concentration is a two-parameter description of the form

$$K_i(\xi, Y_T) = K_0(\xi)\,F\left(\frac{Y_T}{Y_{T_D}(\xi)}\right) \qquad (43)$$

where K_i is the mass fraction of the diffusing species, and Y_{T_D} (ξ) is a measure of the breadth of the mass fraction profile. In this special case it is convenient to take

$$F\left(\frac{Y_T}{Y_{T_D}}\right) = e^{-\frac{Y_T^2}{Y_{T_D}^2}} \tag{43a}$$

Then,

$$\dot{m} = 2(\pi)^m \int_0^\infty \rho u K_i y^m dy = 2(\pi)^m \beta \rho_f u_\infty d^{m+1} K_o Y_{T_D}^{m+1} F_{m+1} = \text{const.} \tag{44}$$

where

$$F_{m+1} = \int_0^\infty \lambda^m e^{-\lambda^2} d\lambda \; ; \; F_1 = \sqrt{\pi/2} \; , \; F_2 = 1/2$$

By introducing a mass flux coefficient, c_m, one has

$$\frac{\rho_f}{\rho_\infty} Y_{T_D}^{m+1} K_o = \frac{\dot{m}_i}{2(\pi)^m \beta \rho_\infty u_\infty d^{m+1} F_{m+1}} = c_m = (\text{constant}) \tag{44a}$$

A second relation between K_o and Y_{T_D} is supplied by the binary diffusion equation, which for $Le_T = 1$ takes the same form as Eq. (27) or (28), with h replaced by K_i.* Along the wake axis (Eq. (34)),

$$\left(\frac{\partial K_i}{\partial \xi}\right)_{Y_T=0} = (m+1)\left(\frac{\partial^2 K_i}{\partial Y_T^2}\right)_{Y_T=0}\left(\frac{\bar{\varepsilon}_T}{\beta u_\infty d}\right) \tag{45}$$

---

* In spite of this fact the normalized mass fraction and enthalpy are not similar during the swallowing process (Section 3), because they do not satisfy the same boundary conditions.

or (Eq. (43a))

$$\frac{dK_c}{d\xi} = -2(m+1)\left(\frac{\tilde{\epsilon}_T}{\beta u_\infty d}\right)\frac{K_o}{Y_{T_D}^2} \tag{45a}$$

For "locally similar" turbulence $\dfrac{\tilde{\epsilon}_T}{\beta u_\infty d}$ is given by Eq. (36); by introducing this relation and Eq. (44a) into Eq. (45a) one obtains

$$K_o^{\left(1+\frac{2}{m+1}\right)}\frac{dK_o}{d\xi} = -\frac{2(m+1)}{C_m^{2/(m+1)}}\frac{\alpha_m^m K(C_{Df})_i}{\beta^2 4^{m+1} G_{m+1}}\left(\frac{\rho(0)}{\rho_f}\right)^{1/(m+1)}\left(\frac{\rho_f}{\rho_\infty}\right)^{2/(m+1)}\left(\frac{\alpha_m \tilde{y}_1}{z_f}\right)\frac{z_f F_1(z_f)}{\left(z_f^{m+1} - \alpha_m^{m+1}\right)} \tag{46}$$

By again taking $\rho \sim p/h$ and integrating, one finds

$$\left(\frac{1}{K_o(\xi)}\right)^{2/(m+1)} - \left(\frac{1}{K_o(\xi_i)}\right)^{2/(m+1)} = \frac{\alpha_m^m K(C_{Df})_i}{\beta^2 4^m G_{m+1} C_m^{4/(m+1)}}\int_{\xi_i}^{\xi} L(\xi)\,d\xi \tag{47}$$

where

$$L(\xi) = \frac{\left(\frac{p_f}{p_\infty}\right)^{1/(m+1)}\left[\left(\frac{p_f}{p_\infty}\right)^{1/(m+1)}\left(\frac{\alpha_m \tilde{y}_f}{z_f}\right)\right] z_f F_1(z_f)}{\left(\frac{h(0)}{h_\infty}\right)^{1/(m+1)}\left(\frac{h_f}{h_\infty}\right)^{1/(m+1)}\left(z_f^{m+1} - \alpha_m^{m+1} c\right)} =$$

$$= \frac{\left(z_f^{m+1} - \alpha_m^{m+1} d\right)^{\frac{1-m}{1+m}} z_f^m F_2(z_f)}{\mathcal{F}(z_f, H)}\left(\frac{p_f}{p_\infty}\right)^{1/(m+1)}$$

When the static pressure (p_f/p_∞) is known and $z_f(\xi)$ is obtained from the quadrature in Eq. (38), all quantities in L (ξ) are also known (Eq. (37)). An alternative form of (Eq. (47)) is given by

$$\left[\frac{K_0(\xi_i)}{K_0(\xi)}\right]^{2/(m+1)} = \frac{Y_{T_D}^2 \left(\frac{\rho_f}{\rho_\infty}\right)^{2/(m+1)}}{\left(Y_{T_D}\right)_i^2 \left(\frac{\rho_f}{\rho_\infty}\right)_i^{2/(m+1)}} = \tag{48}$$

$$1 + \frac{2(C_{D_f})_i \alpha_m^{m+2} K}{\beta^2 4^m G_{m+1} \left(z_f^{m+1} - \alpha_m^{m+1} J\right)_i^{2/(m+1)}} \int_{\xi_i}^{\xi} L(\xi) d\xi$$

where the initial turbulent mass fraction and enthalpy profiles are "matched" by taking $(Y_{T_D})_i^2 = \frac{1}{2}(Y_{T_f})_i^2$ (Appendix 3).

Once the mass fraction is known the value of the number density per unit volume along the axis is calculated from the relation

$$\frac{n_I(\xi_i, 0)}{n_I(\xi, 0)} = \frac{\left(\frac{p_f}{p_\infty}\right)_i \left(\frac{h(0)}{h_\infty}\right)}{\left(\frac{p_f}{p_\infty}\right)\left(\frac{h(0)}{h_\infty}\right)_i} \quad \frac{K_0(\xi_i)}{K_0(\xi)} \tag{49}$$

The number density distribution across the wake is given by

$$\frac{n_I(\xi, Y_T)}{n_I(\xi, 0)} = \frac{\left(\frac{h(0)}{h_\infty}\right)}{\left(\frac{h(Y_T)}{h_\infty}\right)} e^{-Y_T^2/Y_{T_D}^2}, \tag{50}$$

where Y_{T_D} is obtained from Eq. (48).

In the opposite limiting case of "frozen" diffusivity $\frac{\bar{\epsilon}_T}{3u_\infty d}$ is given by Eq. (18a), with $C_{D_f} = (C_{D_f})_i$, and Eq. (45a) becomes (Eq. (44a))

$$K_o^{-(1+\frac{m}{m+1})}\frac{dK_o}{d\xi} = -\frac{2(m+1)}{C_m^{2/(m+1)}}\frac{K\alpha_m^m (C_{Df})_i}{\beta^2 4^{m+1} G_{m+1}}\cdot\left(\frac{\rho_f}{\rho_\infty}\right)^{1/(m+1)}\left(z_f^{m+1} - \alpha_m^{m+1}\delta\right)^{-m/(m+1)} \qquad (51)$$

so that

$$\left(\frac{1}{K_o(\xi)}\right)^{2/(m+1)} - \left(\frac{1}{K_o(\xi_i)}\right)^{2/(m+1)} = \frac{\alpha_m^m K(C_{Df})_i}{\beta^2 4^m G_{m+1} C_m^{2/(m+1)}}\int_{\xi_i}^{\xi}\left(\frac{\rho_f}{\rho_\infty}\right)^{1/(m+1)}\left(\frac{h_f}{h_\infty}\right)^{-1/(m+1)}\left(z_f^{m+1} - \alpha_m^{m+1}\delta\right)^{-m/(m+1)} d\xi \qquad (52)$$

or

$$\left(\frac{K_o(\xi_i)}{K_o(\xi)}\right)^{2/(m+1)} = \frac{Y_{T_D}^2\left(\frac{\rho_f}{\rho_\infty}\right)^{2/(m+1)}}{\left(Y_{T_D}\right)_i^2\left(\frac{\rho_f}{\rho_\infty}\right)_i^{2/(m+1)}} = \qquad (53)$$

$$1 + \frac{2(C_{Df})_i}{\beta^2 4^m}\cdot\frac{\alpha_m^{m+2} K}{G_{m+1}\left(z_f^{m+1} - \alpha_m^{m+1}\delta\right)_i^{2/(m+1)}}\int_{\xi_i}^{\xi}\left(\frac{\rho_f}{\rho_\infty}\right)^{1/(m+1)}\left(\frac{h_f}{h_\infty}\right)^{-1/(m+1)}\left(z_f^{m+1} - \alpha_m^{m+1}\delta\right)^{-m/(m+1)} d\xi$$

In this case $z_f(\xi)$ is obtained from the quadrature for frozen diffusivity (Eq. (39)), and the number density per unit volume is calculated from Eqs. (49), (50), and (53), with the appropriate values of h/h .

According to Eq. (49) the initial decay of number density along the wake axis is caused mainly by the volume expansion of the flow as $p_f \longrightarrow p_\infty$. When $(\xi - \xi_i) \nearrow 50 - 100$, $p_f = p_\infty$, and the cooling of the wake flow, or its increasing density, means naturally that the number density falls off less rapidly with downstream distance than the mass concentration.

As stated before, the swallowing process for the axially-symmetric turbulent inner wake is virtually completed when $(\xi - \xi_i) \sim$ 200, so that $F_2(z_f) \cong 1$ when $(\xi - \xi_i) > 200$. Also

$$z_f^{m+1} >>> \alpha_m^{m+1} \quad \text{AND} \quad \left[K_0(\xi)\right]^{-2/(m+1)} >> \left[K_0(\xi_i)\right]^{-2/(m+1)}$$

By comparing Eqs. (37) and (47), one sees that

$$\left(\frac{f_f}{f_\infty}\right)^{2/(m+1)} Y_{T_D}^2 \cong Y_{T_f}^2 = \left(\frac{f_f}{f_\infty}\right)^{2/(m+1)} Y_{T_\infty}^2 ,$$

or

$$Y_{T_D}^2 \cong Y_{T_f}^2 .$$

As expected, the normalized mass fraction and complete static enthalpy are similar once the swallowing process is completed. Thus

$$\frac{f_+}{f_-} K_0(\quad) \sim \quad^{-\left(\frac{n+1}{n+2}\right)}$$

(Similar remarks are applicable also to the case of "frozen" diffusivity.)

This slow decay of peak concentration along the axis represents the limiting case of zero or "slow" recombination rate. If the diffusing species is reactive, the equilibrium concentration ("very fast" reaction rates) is a function of the temperature and pressure, and is known once the enthalpy field is known (Section 3.1.). The actual distribution of the diffusing species along the wake axis lies between these two extremes, and the methods of the present paper can be generalized to include finite recombination rates whenever these rates are known.

4. Distribution of Some Observables in the Wake: Comparison with Experiment

4.1. Inviscid Enthalpy Profiles for Axially-Symmetric Flow and Initial Conditions for Inner Wake

Two examples have been calculated in detail for axially-symmetric flow: (1) $M_\infty = 8.5$ and $p_\infty = 1$ ATM, corresponding to the conditions for most of the experimental data on wake growth obtained in ballistic ranges; (2) $M_\infty = 22$ at an altitude of 100,000 feet, corresponding to typical ballistic reentry conditions. The calculations were divided into three different regions, beginning at the wake neck and moving downstream. First, a very short region was assumed to occur in which pure expansion (no mixing) takes place because of the rapid drop in pressure immediately behind the wake shock. This effect is so predominant that it overrides any mixing that could occur until the pressure is 3-4 times ambient. In that region the entire flow field was expanded simply by the volume ratio required to reduce the neck pressure to the initial mixing pressure, which was assumed to occur at $p = 4p_\infty$. (The fact that pressure heavily dominates at first and then mixing gradually begins to take hold is brought out clearly by the wake growth results.) The second region extends from the station where $p = 4p_\infty$ to the point at which the pressure becomes ambient. In this region both pressure drop and mixing occur. In the third and final region the pressure is ambient everywhere and mixing alone needs to be considered.

It is necessary to determine the neck pressure and fix its decay to ambient conditions. Characteristics calculations were carried out at $M_\infty = 22$ for the geometry shown in the sketch below using the Wohlwill[13] computer program. Briefly, the pressure p_2 (see sketch) immediately behind the wake shock, which depends on Mach number, is about $24p_\infty$ for $M_\infty = 22$ ($p_2 \sim 7.5\ p_\infty$ for $M_\infty = 8.5$), and the pressure drops to a value four times ambient in a distance of about six body diameters behind the wake shock (only one diameter is required at $M_\infty = 8.5$). Since $\tilde{y}_{f_{neck}} \doteq .18$ for these conditions, the turbulent core expands by a factor

$$\left(\frac{p_2}{4\ p_\infty}\right)^{\frac{1}{2}} \doteq \sqrt{6}$$

to a value $\tilde{y}_{f_i} = .44$ in this initial region before mixing begins ($\tilde{y}_{f_i} = .25$ at $M_\infty = 8.5$). Assuming the neck position to be about

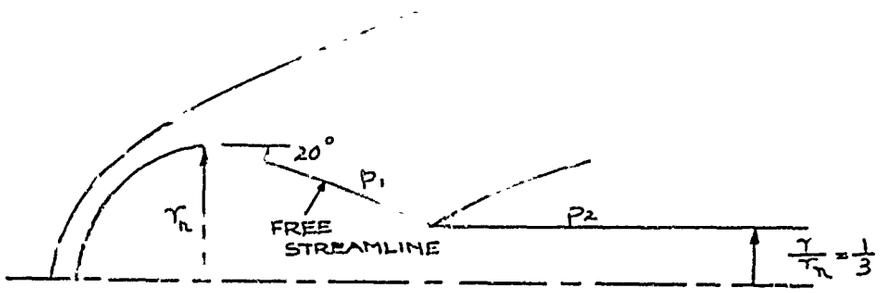

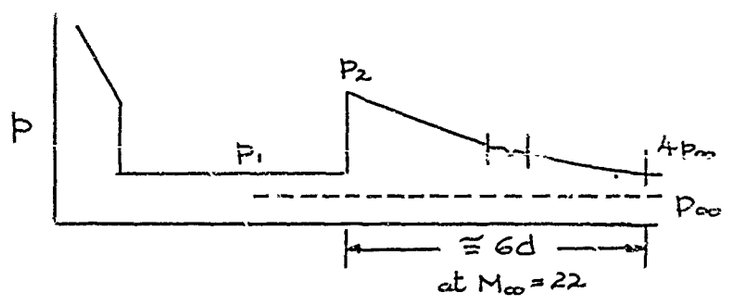

1.5 body diameters behind the nose, the initial stations measured from the nose where mixing calculations were begun were $x/d = 7.5$ for $M_\infty = 22$ and $x/d = 2.5$ for $M_\infty = 8.5$. The distance downstream to the point where the pressure returns to ambient is also a function of the free stream Mach number. For $M_\infty = 8.5$, $(x/d)_{p = p_\infty} \cong 25$ and for $M_\infty = 22$, $(x/d)_{p = p_\infty} \cong 50$.

At the initiation of mixing, the inviscid enthalpy profile in the outer wake must be specified. Since the enthalpy is relatively insensitive to pressure in the range $1 \leq p/p_\infty \leq 4$ the enthalpy profile corresponding to ambient pressure is employed in the calculations. To find the inviscid enthalpy profile at $p = p_\infty$ the shape of the bow shock was used as described in Appendix 1. If the shape is known analytically and γ is approximated, an analytical expression for the downstream profile can be found, as shown by Lykoudis[14]. Alternatively, if the entropy distribution behind the shock is found, the profile at $p = p_\infty$ can be determined numerically by continuity methods, as described by Goulard[15]. In the present paper the continuity method was used at $M_\infty = 8.5$ and both methods were employed for $M_\infty = 22$. The resulting profiles when transformed to the Howarth-Dorodnitsyn variable by Eq. (1) are shown in Figures 5 and 6.

At the axis the slope of the profile must be zero, as shown in Appendix 1. Since the numerical and analytical shock shapes used

for $M_\infty = 22$ all agree fairly well in the body nose region (Appendix 1, Figure 19), the enthalpy profiles also agree quite well near the axis. Away from the axis the parabolic shock gives a higher enthalpy because the slope of this shock surface is somewhat steeper. For computational purposes the enthalpy profiles were approximated by combining a Gaussian curve near the axis with an exponential curve in the outer portion, in such a manner that the total drag coefficient was unity, and the slopes of the two curves agreed at the matching point. It should be emphasized that this procedure was employed for convenience only, and exact values from the profiles could be used just as well. It was found from the computer program described previously that the wake shock raises the value of the enthalpy along the stagnation streamline by 5 per cent. Combining these features gives the following equations for the enthalpy, which are also shown in Figures 5 and 6.

$$M_\infty = 8.5 \quad \left(z = \alpha_m Y_L = 1.722\, Y_L\right)$$

$$z \leq .5$$

$$\left(\frac{h}{h_\infty} - 1\right) = 4.2\, e^{-z^2} \tag{54a}$$

$$z \geq .5$$

$$\left(\frac{h}{h_\infty} - \quad , = 5.39 e^{-z}\right. \tag{54b}$$

$$M_\infty = 22 \quad \left(z = \alpha_m Y_L = 1.922\, Y_L\right)$$

$$z \leq .5$$

$$\left(\frac{h}{h_\infty} - 1\right) = 38.84\, e^{-z^2} \tag{55a}$$

$$z \geq .5$$

$$\left(\frac{h}{h_\infty} - 1\right) = 49.87\, e^{-z} \tag{55b}$$

Based on the estimates described in Appendix 4, the values of the initial drag contained in the turbulent core were taken as follows:

M_∞	$(C_{D_f})_i$
8.5	.022
22.0	.0077

The effect of different values of $(C_{D_f})_i$ on the resultant wake growth is considered later for one of the examples. The experimental constant, K, used in the diffusivity was taken as 0.04 (Appendix 3). Also, the value of β (Eq. 12) was taken to be 0.9.

4.2. Turbulent Diffusivity

The growth of the turbulent diffusivity for "locally similar" turbulence has been discussed in a general way in Section 2; we now examine the numerical results for $M_\infty = 8.5$. The exact expression for $\widetilde{\epsilon}_T Y_{T_f}^m$ can be obtained from Eqs. (13) and (33) and is given by

$$\frac{\widetilde{\epsilon}_T Y_{T_f}^m}{\iota_\infty \beta d} = \frac{K \alpha_m (C_{D_f})_i \left(\frac{h_f}{h_\infty}\right) \tilde{y}_f F_1(z)}{\beta^2 4^{m+1} G_{m+1} \left(\frac{p_f}{p_\infty}\right)^{m/(m+1)} \left(\frac{h(0)}{h_\infty}\right)^{1/(m+1)} \left(z^{m+1} - \alpha_m^{m+1} \delta\right)^{1/(m+1)}} \quad (56)$$

This quantity compared to its initial value is shown in Figure 7 as a function of downstream distance from the initial mixing station. The rapid initial growth in $\widetilde{\epsilon}_T Y_{T_f}^m$ is caused by the pressure decrease and accompanying rapid increase in $\tilde{y}_f$. The region $x/d \cong 10 - 20$ illustrates the early stages of mixing before the diffusivity increases rapidly again. The explosive growth of diffusivity begins at $x/d \cong 40$ for the condition shown. For two-

dimensional flow and the same external conditions this growth would occur much later. According to Figure 7 the process of swallowing enthalpy or momentum defect originally contained in the outer wake is virtually completed in about 300 body diameters. Far downstream the diffusivity approaches the asymptotic value given by the relation

$$\frac{\bar{\epsilon}_T}{\beta u_\infty d}\, Y_{T_{\frac{1}{2}}}^{m} = \frac{K}{\beta^2 4^{m+1} G_{T_{m+1}}} \left[C_{D_o} + \left(C_{f}\right)_i \right]$$

4.3. Growth of the Turbulent Inner Wake

The calculated growth of the turbulent inner wake at a flight velocity of 9,500 ft./sec. is shown in Figure 8 for both "locally similar" turbulence and "frozen" diffusivity. Up to x/d = 15-20 the two limiting cases are practically identical, because the marked increase in turbulent diffusivity in the "locally similar" case has not yet begun (Figure 7), and the pressure drop plays an important role. Downstream of this region the "locally similar" wake grows rapidly to a width of about 3 body diameters at x/d = 100, 5 body diameters at x/d = 300, and 8 body diameters at x/d = 1,000. Soon after the swallowing process is completed ($x/d > 300$) the wake width approaches the familiar 1/3-power growth curve corresponding to the total drag of the body. Wake widths calculated on the assumption of "frozen" diffusivity are smaller by a factor of at least two over the range $200 < x/d < 4{,}000$.

These calculations are compared with experimental shadowgraph data

in Figure 9. Most of the data are supplied by Slattery[16] and Clay (9,000 ft./sec.) at the Lincoln Laboratory (M.I.T.). Some additional points obtained in the region $x/d < 300$ were taken from Feldman[2] (AVCO) (15,000 ft./sec.) and Dana[17] and Short (CONVAIR) (7,400 ft./sec.). The experimental scatter is too large to detect any details of a rapid growth region in the early stages ($x/d < 50$). The most important result is that the predicted growth of the inner wake for "locally similar" turbulence is in good agreement with the shadowgraph measurements in the range $200 < x/d < 4,000$, while the wake widths calculated for "frozen" diffusivity are too low by a factor of about two. No adjustment of the diffusivity constant K was necessary to fit the data.

The theory (Section 3) indicates a weak dependence of wake width on flight velocity, and agrees qualitatively with the fact that Feldman's data obtained at 15,000 ft./sec. lies in general above the computed curve (Figure 9), while the data of Dana and Short at 7,400 ft./sec. lie below the curve.

At a flight velocity of 22,000 ft./sec. the calculations show that the inner wake grows more rapidly in the region $x/d < 300$ than at 9,500 ft./sec. (Figures 10 and 11), because of the combined effect of a larger pressure drop and a higher effective turbulent diffusivity. However, the wake grows more slowly than the 1/3-power during some

region $x/d > 300 - 400$, because the core is still much hotter than ambient (Eq. (37e)). The enthalpies along the axis and the front are shown in Figure 12. At $\frac{x}{d} = 1{,}000$ the axis enthalpy is still over six times ambient. In fact, the calculated curve of wake growth has not yet taken on the 1/3-power behavior at $x/d = 4{,}000$. Of course very far downstream the wake boundaries for all flight velocities must eventually coincide (for the examples shown this occurs at $\frac{x}{d} > 10^5$) if the total body drag coefficient is the same.

4.4. Effect of $(C_{D_f})_i$

In order to determine how accurately the value of $(C_{D_f})_i$ must be known, calculations were made at $M_\infty = 22$ for two values of initial drag differing by a factor of two, namely .0077 and .0155. The enthalpy increment on the axis of the inner wake was taken to be the same for both values of $(C_{D_f})_i$. According to Eqs. (A.2-8) and (37d), if

$$(B_1/H)_{.0077} = (B_1/H)_{.0155}$$

then the quantity

$$(B_1/H) = \frac{q_{m+1}}{C_{D_o} \cdot G_{m+1}} \quad \frac{F_1(z)}{\left(\frac{z_f^{m+1}}{(C_{D_f})_i} - \frac{(m+1)\,q_{m+1}}{C_{D_o}} \cdot \frac{H}{H+1}\right)}$$

is also the same. In taking $B_1 = \text{const.}$ we must have the ratio $\frac{(z_f)^{m+1}}{(C_{D_f})_i} = \text{constant}$; thus if $(C_{D_f})_i$ is doubled z_{f_i} must increase

by $\sqrt{2}$. Then the initial fronts are not quite at the same position and neither $\frac{h(0)}{h_\infty}$ or $\frac{h_f}{h_\infty}$ have the same values. This discussion shows that the value of z_{f_i} must be chosen to be consistent with $(C_{D_f})_i$ and $(B_1/H)_i$.

The growth of the turbulent inner wake is shown in Figure 13 for initial values of the drag coefficient equal to .0077 and .0155 with and without pressure effects. The axial coordinate is measured from the initial mixing station. Differences in downstream location for a given wake width are large in the initial stages ($x/d < 100$), but soon become unimportant once the swallowing process is in full swing. For these two cases, the values of the integrand of Eq. (38), $\mathcal{F}(z_f, H)$, were essentially identical after $x/d = 125$. The differences in this function occur only for small z_f and upon integration eventually become a small contribution.

Here the effect of the pressure drop in shaping the early portions of the front is very evident, resulting in a parabolic behavior as opposed to the slow initial growth predicted by mixing alone.

4.5. Mass Diffusion Calculations

Calculations for turbulent mass diffusion at $M_\infty = 22$ are shown in Figure 14. As described in Section 3.2, this case represents the limiting behavior in which some species is contained entirely within

the inner wake, and no recombination occurs, so that the total number of particles remains the same. The behavior with "locally similar" turbulence and "frozen" diffusivity is shown as computed from Eqs. (48), (49), and (53). A rapid decrease in concentration occurs first, because of the pressure drop, but by x/d = 500 the peak concentration along the axis is falling slowly because of the slow growth of the wake width and the cooling effect (Figures 10 and 11). In these calculations, the pressure drop accounts for a decrease by about a factor of five while the mixing accounts for about two orders of magnitude up to x/d = 1,000. The values of peak concentration for "frozen" diffusivity are almost an order of magnitude above the values for "locally similar" turbulence.

4.6. Electron Distribution

Electron concentrations in the wake can be found from the enthalpy and pressure distributions. Representative results are shown in Figures 15, 16, and 17. In these illustrative examples it is assumed that the flow is in complete thermodynamic equilibrium at least up to the neck location. The lower curve in Figure 15 shows the axial distribution of electrons for M_∞ = 22 at 100,000 ft., assuming that the electrons also follow the equilibrium flow conditions in the wake given by the "locally similar" turbulence calculations. Here the initial concentration is equal to the value at the neck, or in other words, it is given by the conditions $\frac{h\,(0)}{h_\infty} = .6\ \frac{h_{\text{stagnation}}}{h_\infty}$ and $p = 24\ p_\infty$.

The pressure drop to ambient has a strong influence for a short distance, after which $\frac{h\,(0)}{h_\infty}$ determines the distribution. The distribution crosses the equivalent C-band (5600 mc/sec; $n_e \cong 3.1 \times 10^{11}/cm^3$)* electron concentration at $x/d \cong 100$, L-band (1300 mc/sec; $n_e \cong 1.7 \times 10^{10}/cm^3$) at $\frac{x}{d} \cong 200$, and the lowest frequency, UHF (400 mc/sec; $n_e \cong 1.6 \times 10^9/cm^3$), at $x/d \cong 325$.

The curve in Figure 15 labelled "pure diffusion" corresponds to the case of frozen flow in the wake so far as the electrons are concerned. The initial conditions are the same as for the equilibrium case, but the presence of electrons in the outer wake is ignored. Thus the normalized distribution of number density is identical with the diffusion results shown in Figure 14. Again the pressure drop in the initial region accounts for a considerable portion of the decrease in n_e. In fact the differences between the two limiting cases of frozen and equilibrium flow are not large for $x/d < 100$. Downstream of $x/d = 150$ the electron concentration is

---

* In rationalized units, the electrons $/cm^3$ are given by $n_e = \frac{m_e \epsilon_o}{e^2} \omega^2 \cong \frac{f^2}{10^8}$ where ω and f are radar frequencies in radians and cycles per second respectively, ϵ_o is the dielectric constant of free space, and e and m_e are the electronic charge and mass respectively. We consider here the lengths to be roughly the distance between the object and the position where the electron density falls below the value given by this equation for any radar frequency.

orders of magnitude larger in the case of pure diffusion, as expected. As discussed in Section 3.2, these two cases should represent the limits of behavior, and the actual situation lies between these two limits.

The third curve in Figure 15 shows the axial electron distribution for the laminar equilibrium condition as calculated by Feldman[2] and Lykoudis.[14] The strong pressure effect initially is similar, but once the pressure is ambient ($\frac{x}{d} > 100$) the slow time scale compared with turbulent diffusion is evident.*

In Figure 16 the calculations have been scaled to an altitude of 200,000 ft. for illustrative purposes. Here the equilibrium conditions would indicate no C-band wake. The L-band wake length corresponds to a value of $\frac{x}{d} \cong 50$, while the trail length for UHF corresponds to $\frac{x}{d} \cong 150$. However, the pure diffusion wake would have a UHF length of $x/d \cong 250$.

Finally, the radial distribution of electrons at several axial stations is shown in Figure 17 for $M_\infty = 22$ and $h_\infty = 100{,}000$ ft.,

---

* The laminar calculations do not account for the initial heated inner core, hence the difference in the concentrations for $\frac{x}{d} < 100$.

under the assumption of equilibrium and "locally similar" turbulent flow conditions. Near the neck the electrons appear restricted to a fairly narrow region, but they diffuse outward rapidly downstream of the neck. The total width of the plasma cylinder corresponding to the plasma frequency at L-band remains virtually constant in the region $30 < x/d < 110$ at about 3.5 body diameters. The width corresponding to UHF remains practically constant at about 5.5 body diameters in the region $30 < x/d < 250$.

5. Conclusions and Future Work

1. At velocities of the order of 9,000 - 10,000 ft./sec., the predicted growth of the inner wake for "locally similar" turbulence is in good agreement with shadowgraph measurements of wakes behind spheres obtained in ballistic ranges. Wake widths calculated for the opposite limiting case of a "frozen" diffusivity determined only by the initial drag of the inner wake are too small by a factor of at least two over the range $200 < x/d < 4,000$ covered by the experimental data. We conclude that the adjustment time for the scale and intensity of turbulence must indeed be short compared to the time scale for the changes in turbulent diffusivity along the wake axis. The adjustment is probably made easier by the fact that the process of swallowing enthalpy or momentum defect originally contained in the outer wake is almost completed in about 300 body diameters. The constant K appearing in the expression for turbulent diffusivity in the present paper corresponds directly to Townsend's "universal" Reynolds number R_T for low-speed turbulent wakes. Tentatively one concludes that the turbulence mechanism in the wake with respect to a fixed observer is probably quite similar to the low speed case, in spite of the large mean temperature gradients. Experimental studies of the structure of turbulence in the wake are required to settle this point.

Measurements of the growth of the turbulent inner wake behind blunt-nosed bodies of various nose bluntness ratios at velocities

of the order of 20,000 ft./sec. would help to clarify the influence of the nose drag, the outer wake enthalpy distribution, and the hot core in the inner wake.

2. Once the swallowing process is in full swing the influence of the initial drag coefficient $(C_{D_f})_i$ is small, because the drag absorbed from the outer inviscid wake is so much larger than the initial drag. However, the "incubation length" required for the inner wake to begin swallowing momentum defect at an appreciable rate is proportional to $(C_{D_f})_i^{-1/3}$ in the two-dimensional case, and to $(C_{D_f})_i^{-1/4}$ in the axially-symmetric case. A brief analysis shows that $(C_{D_f})_i$ varies with Reynolds number like $(Re)^{-\frac{1}{2}}$ when the free shear layer is laminar, and a rough estimate establishes the value of $(C_{D_f})_i$ within a factor of about two. Careful theoretical and experimental studies of the re-compression just behind the body are required if the initial conditions for the turbulent inner wake are to be specified more precisely.

Theoretical investigations of the stability of laminar flow in the wake, and extension of hot-wire studies of laminar-turbulent transition in the axially-symmetric wake would be very helpful in determining the lower Reynolds number limit for the appearance of turbulence.

3. Because the fluid in the free shear layer above the zero stream-line is decelerated and compressed at the "neck", the gas in the inner

wake is much hotter initially than the gas in the outer wake at the turbulent front. In one typical example ($M_\infty = 22$, h = 100,000 ft.) the enthalpy along the wake axis requires a distance of about 150 body diameters to cool down to a value equal to the initial enthalpy in the outer wake at the front. Even at x/d = 1000 the enthalpy on the wake axis is still about 10 times ambient for a blunt body such as a sphere. The axial variation of the enthalpy at the front ($\tilde{y} = \tilde{y}_f$) is simply a one-to-one mapping of the curve of wake growth $\tilde{y}_f(\xi)$ on the original enthalpy distribution in the outer wake.

4. As an example of turbulent mass diffusion the decay of peak electron density along the axis of the inner wake is calculated for $M_\infty = 22$, h = 100,000 ft., on the assumption that the initial electron density corresponds to thermodynamic equilibrium, and that the electron-ion recombination rate in the wake is negligibly small. The peak electron density decays from a value of $5 \times 10^{13}/cm^3$ to a value corresponding to the plasma frequency at L-band (f = 1300 mc/sec; $n_e \tilde{=} 1.7 \times 10^{10}/cm^3$) in a downstream distance of about 1000 body diameters. This length should be compared with the corresponding distance of about 200 body diameters for complete thermodynamic equilibrium (very fast recombination rates). The actual situation is expected to lie somewhere between these two limits. In any event the predicted radar trail length for a blunt body is fairly long, even with turbulent diffusion.

One interesting result for equilibrium flow at $M_\infty = 22$ and h = 100,000 ft. is that the width of the plasma cylinder corresponding to the plasma frequency at L-band remains virtually constant at about 3.5 body diameters in the region $30 < x/d < 110$, while the width corresponding to UHF (400 mc/sec; $1.6 \times 10^9/cm^3$) remains practically constant at about 5.5 body diameters in the region $30 < x/d < 250$.

Similar calculations can be carried out for equilibrium gas radiation intensity or radiation from an ablating species in the wake.

5. The results obtained in the present paper are sufficiently encouraging so that one can begin to think of including the effects of chemical and electron-ion recombination processes. Clearly these rate processes and turbulent diffusion interact when streamlines enter the spreading inner wake, because of the effect of diffusion on the local mass fractions of the reacting species. Hopefully, the methods utilized by S. C. Lin [18] and J. D. Teare (and others) for the outer wake can be combined with the present analysis to give a more complete picture of the wake at hypersonic speeds.

ACKNOWLEDGMENTS

The authors wish to express their appreciation to Dr. Richard Slattery (Lincoln Lab) and Dr. Wallace Short (Convair) for making available to us their unpublished data on wake growth. We also wish to thank the following: Dr. Hans Wohlwill and Mr. Garth Lippman who helped in the computer calculations, Miss Gina Ferlan for making the hand calculations and the two typists, Mrs. Verna Ankerman of STL and Mrs. Geraldine Van Gieson of GALCIT.

REFERENCES

1. Lin, S. C.: Cylindrical Shock Waves Produced by Instantaneous Energy Release. Journal of Applied Physics, Vol. 25, No. 1, pp. 54-57, January, 1954.

2. Feldman, S.: On Trails of Axi-Symmetric Hypersonic Blunt Bodies Flying through the Atmosphere. AVCO-Everett Research Laboratory, Research Report No. 82, December, 1959. Also, Journal of the Aerospace Sciences, Vol. 28, No. 6, pp. 433-448, 470, June, 1961.

3. Demetriades, A.: Some Hot-Wire Anemometer Measurements in a Hypersonic Wake. 1961 Heat Transfer and Fluid Mechanics Institute, University of Southern California, June 19-21, 1961.

4. Chapman, D. R.; D. M. Kuehn; H. K. Larson: Investigation of Separated Flows in Supersonic and Subsonic Streams with Emphasis on the Effect of Transition. NACA Report No. 1356, 1958. (Supersedes NACA TN 3869).

5. Larson, H. K. and S. J. Keating, Jr.: Transition Reynolds Numbers of Separated Flows at Supersonic Speeds. NASA TN D-349. December, 1960.

6. Townsend, A. A.: The Structure of Turbulent Shear Flow. especially Chapter 7, Cambridge University Press, 1956.

7. Lees, L.: Convective Heat Transfer with Mass Addition and Chemical Reactions. Third AGARD Colloquium on Combustion and Propulsion, pp. 451-498, Pergamon Press, March, 1958.

8. Reynolds, O.: On the Extent and Action of the Heating Surface of Steam Boilers. Collected Papers, Vol. 1, pp. 81-85.

9. Hall, A. A. and G. S. Hislop: Velocity and Temperature Distributions in the Turbulent Wake behind a Heated Body of Revolution. Proc. Cambridge Phil. Soc., Vol. 34, pp. 345-350, 1938.

10. Mager, A.: Transformation of the Compressible Turbulent Boundary Layer. Journal of the Aeronautical Sciences, Vol. 25, No. 5, pp. 305-311, May, 1958.

11. Ting, L. and P. A. Libby: Remarks on the Eddy Viscosity in Compressible Mixing Flows. Journal of the Aeronautical Sciences, Vol. 27, No. 10, pp. 797-798, October, 1960, (Readers' Forum).

REFERENCES (Cont'd.)

12. Goldstein, S. (editor): Modern Developments in Fluid Dynamics, Vol. 2, Oxford University Press, 1938, especially Chapter 13, pp. 571-577.

13. Wohlwill, H. E.: Formulation for Machine Computing of Axi-Symmetric Supersonic Flow. STL GM-TN-56, Revision 1, November 14, 1957.

14. Lykoudis, P. S.: Ionization Trails. The Rand Corporation, Report No. P-2244, March, 1961.

15. Goulard, M.: The Accuracy of Characteristics Calculations. Private Communication.

16. Slattery, R. E., and W. G. Clay: Width of the Turbulent Trail Behind a Hypervelocity Sphere. Massachusetts Institute of Technology, Lincoln Laboratory Report No. 35 G-0004, June, 1961.

17. Dana, T. A. and W. W. Short: Experimental Study of Hypersonic Turbulent Wakes. Convair, Report No. ZPh-103, May, 1961.

18. Lin, S. C., and J. D. Teare: A Streamtube Approximation for Calculation of Reaction Rates in Inviscid Flow Field of Hypersonic Objects. AVCO-Everett Research Laboratory, Research Note No. 223, April, 1961.

19. Goulard, M., and R. Goulard: The Aerothermodynamics of Re-entry Trails. Presented at the ARS Semi-Annual Meeting, May 9-12, 1960, ARS Preprint 1145-60, May, 1960.

20. Van Hise, V.: Analytic Study of Induced Pressure on Long Bodies of Revolution with Varying Nose Bluntness at Hypersonic Speeds. NASA Report No. TR-R-78, Advance Copy, May, 1960.

21. Wohlwill, H. E.: The Stream Function Equation for a High-Temperature Gas in Axi-Symmetric Rotational Flow. STL GM-TM-0165-00100, December, 1957.

22. Lees, L.: Recent Developments in Hypersonic Flow. Jet Propulsion, Vol. 27, No. 11, pp. 1162-1178, November, 1957.

23. Dewey, C. Forbes Jr.: GALCIT Hypersonic Research Project, Quarterly Status Report No. 22, January 1 to April 1, 1961.

APPENDIX I

ENTHALPY DISTRIBUTION IN THE OUTER WAKE

We consider the inviscid flow region for $\frac{x}{d} > 25\text{-}50$ where the static pressure is virtually equal to the ambient pressure. The enthalpy profile is independent of axial distance and is specified by the bow and wake shock shapes. The procedure used here to calculate the profile is to determine the profile that would exist for a semi-infinite hemisphere-cylinder, and then modify this profile slightly to correct for the wake shock. Feldman[2] has shown that this correction is small and for many applications could be neglected.

If the bow shock shape is known analytically and γ is approximated, an analytical expression for the downstream profile at ambient pressure can be found, as shown by Lykoudis.[14] Alternatively, given a numerical shock shape, the mass flux and entropy distributions just downstream of the shock can be found. Assuming an isentropic expansion to ambient pressure some distance downstream of the nose, the flow variables can be found corresponding to the ambient pressure and the entropy values downstream of the shock. The radial position or distribution of the streamlines is determined by a continuity balance for the mass flux entering the bow shock along any given streamline. Goulard[15] first applied this method as a means of comparing various flow field techniques.

Thus the problem is basically that of determining the correct shock shape. Feldman[2] used the method of characteristics and computed downstream to $\frac{x}{d} \cong 25$ along the hemisphere-cylinder. These values were subsequently used by himself and the Goulards[19] to solve the laminar heat conduction problem in an equilibrium wake flow. However, as Goulard[15] pointed out, the characteristics method is subject to accumulative errors when it is extended to the downstream distances needed. The present authors have had the same experience with computer calculations run in conjunction with this investigation. Considerable care in the programming procedure is necessary.

Blast wave theory indicates that a parabolic shock should exist. Lykoudis[14] has used this fact with the decided advantage that a closed solution was obtained even to the laminar conduction problem. There are two features which modify this assumption: (1) Because of the entropy layer, a parabolic shock can not exist for a hemisphere-cylinder* and the exponent must be slightly less than .5. This result has also been found by Van Hise[20], who used the sonic cone method and obtained computer solutions to various body shapes. He found the shock shapes for all the various bodies could be correlated very well by the equation

$$\frac{\Delta}{d} = .98\left(\frac{x}{d}\sqrt{C_D}\right)^{.46} \qquad \text{(A.1-1)}$$

(2) Real gas effects (the Van Hise computer calculations were for constant γ) can be important. The density no longer has the given

*This fact was recently pointed out to us by Dr Milton Van Dyke

maximum ratio $\frac{\gamma+1}{\gamma-1}$ across the shock, and the shock shape is modified accordingly.

Regarding the correction for the secondary shock, it has been found that the body streamline enthalpy when expanded to p_∞ is raised by about 5% over that on the hemisphere-cylinder surface. The amount in axially-symmetric flow can be somewhat different from that for two-dimensional flow, since the free expansion streamline behind the body in the former case tends to curve inward as the axis is approached, resulting in a different secondary shock strength.

For the specific examples used in the present work, the experimental shock shapes shown in Figure 18 were employed to get the entropy and mass distribution for $M_\infty = 8.5$. The entropy distribution downstream of this shock was found using the Wohlwill[13] computer shock routine, and then the continuity balance described before was used to get the profile at $p = p_\infty$. At $M_\infty = 22$ the Wohlwill[13] computer program was used to get the subsonic and transonic shock shapes. The result at $M_\infty = 22$ is shown in Figure 19 compared with the shock shapes given by the Van Hise[20] and Lykoudis[14] equations. For both examples, the final enthalpy profiles when transformed by the Howarth-Dorodnitsyn variable are shown in Figures 5 and 6.

The laminar profile exhibits a flat region near the axis followed by a rather rapid drop in enthalpy. Since this shape contributes to

the initially slow and then explosive growth of the turbulent mixing, one should examine theoretically whether the initial slope at the axis is finite or indeed zero. This point can be investigated by using the procedure given by Wohlwill[21] for calculating the gradients normal to a streamline crossing a shock. We first calculate the entropy gradient,

$$T_s \frac{dS}{d\psi} = T_s \frac{dS}{d\phi} \frac{d\phi}{d\psi} \tag{A.1.2}$$

where ψ is the stream function, T_s is the temperature behind the shock and ϕ is the shock inclination angle measured from the axis. Since

$$T_s dS = dh - \frac{dp}{\rho} \tag{A.1.3}$$

and from the Rankine - Hugoniot relations

$$h = h_\infty + \tfrac{1}{2} u_\infty^2 \sin^2\phi \left[1 - \left(\frac{\rho_\infty}{\rho}\right)^2\right] \tag{A.1.4}$$

$$p = \rho_\infty u_\infty^2 \sin^2\phi \left(1 - \frac{\rho_\infty}{\rho}\right) + p_\infty$$

it follows that

$$T_s \frac{dS}{d\phi} = u_\infty^2 \sin\phi \cos\phi \left[1 - \frac{\rho_\infty}{\rho}\right]^2 \tag{A.1.5}$$

so

$$T_s \frac{dS}{d\psi} = u_\infty^2 \sin\phi \cos\phi \left(1 - \frac{\rho_\infty}{\rho}\right)^2 \frac{d\phi}{d\psi} \tag{A.1.5a}$$

We want

$$T_s \frac{dS}{dr} = T_s \frac{dS}{d\psi}\frac{d\psi}{dr} = u_\infty^2 \sin\phi\cos\phi\left(1-\frac{\rho_\infty}{\rho}\right)^2 \frac{d\phi}{dr} \tag{A.1.5b}$$

For two-dimensional flow,

$$\rho_\infty u_\infty dR = \rho u dr \tag{A.1.6a}$$

and for axially-symmetric flow,

$$\rho_\infty u_\infty R dR = \rho u r dr \tag{A.1.6b}$$

where the notation is shown in the sketch.

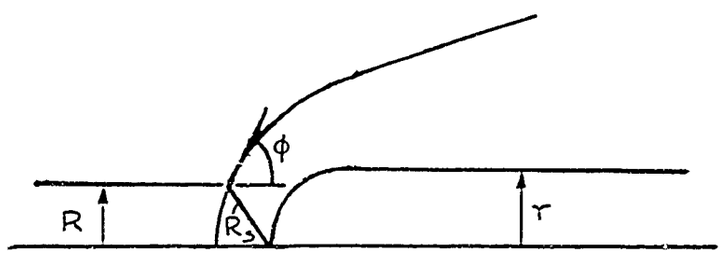

Now $\frac{dS}{d\psi}$ is a constant along any streamline. Since the pressure is constant, TdS = dh and we have finally for two-dimensional flow

$$T\frac{dS}{dr} = \frac{dh}{dr} = \frac{T(\rho u)u_\infty^2 \cos\phi\left(1-\frac{\rho_\infty}{\rho}\right)^2}{T_s(\rho_\infty u_\infty)R_s} \tag{A.1.7a}$$

and axially-symmetric flow

$$T\frac{dS}{dr} = \frac{dh}{dr} = \frac{T(\rho u)r\,u_\infty^2\left(1-\frac{\rho_\infty}{\rho}\right)^2}{T_s(\rho_\infty u_\infty)R_s^2} \tag{A.1.7b}$$

Since $\phi = 90^\circ$ for the stagnation streamline, the normal entropy and enthalpy gradients are always zero for two-dimensional flow regardless of the body shape. For axially-symmetric flow, the gradient is

proportional to the body radius r, and is zero only if the streamline returns to the axis, which it does in the present case. Thus the enthalpy gradient at the axis is zero.

Finally, with the enthalpy profile of the form given by Eq. (2)

$$\left(\frac{h_L}{h_\infty}-1\right)=\left(\frac{h_L}{h_\infty}-1\right)_o g(\alpha_m Y_L) = Hg(z) \qquad (2)$$

the value of α_m can be found from the drag coefficient C_{D_o}. When $(h - h_w) \cong \frac{1}{2}\rho_\infty u_\infty^2$ the drag coefficient is given by the expression

$$C_{D_o} = \frac{4^{m+1}}{\rho_\infty u_\infty^2 d^{m+1}} \int_o^\infty \rho u(u_\infty - u) y^m dy \qquad (A.1.8)$$

where $D_o = C_{D_o}\left(\frac{\rho_\infty u_\infty^2}{2}\right)\frac{(\pi)^m d^{m+1}}{4^{m+1}}$. Since $h - h_{co} \cong -\beta u (u - u_{co})$ and $u \cong \beta u_\infty$

$$C_{D_o} = \frac{4^{m+1} H}{(\gamma-1) M_\infty^2} \int_o^\infty g(\alpha_m Y_L) Y_L^m dY_L \qquad (A.1.8a)$$

$$= \frac{4^{m+1} H}{(\gamma-1) M_\infty^2 \alpha_m^{m+1}} \int_o^\infty g(z) z^m dz$$

Hence

$$\alpha_m^{m+1} = \frac{4^{m+1} H g_{m+1}}{(\gamma-1) M_\infty^2 C_{D_o}} \qquad (A.1.9)$$

with

$$g_{m+1} = \int_o^\infty g(z) z^m dz \qquad (A.1.10)$$

APPENDIX 2

RELATION BETWEEN INVISCID AND TURBULENT MASS FLUX QUANTITIES $Y_{L_f}^{m+1}$ AND $(\rho_f/\rho_\infty)\, Y_{T_f}^{m+1}$

The rate of entrainment of mass flux by the inner wake is given by the expression

$$\frac{d\dot{m}_f}{dx} = \rho_f u_f \left(\frac{dy_f}{dx} - \beta_f \right) \qquad \text{(A.2-1)}$$

where β_f is the inclination of the streamline just entering the inner wake. In the present analysis the influence of the turbulent inner wake on the outer wake is regarded as a second-order effect (Section 2). In other words, ρ_f, u_f, and β_f are supposed to have the same values along the curve $y = y_f(x)$ as they would have if the outer wake flow field extended smoothly to the axis. To this approximation Eq. (A.2-1) states that the rate of increase of mass flux $\dot{m}_f$ contained within the bounding curve $y = y_f(x)$ is also the same; therefore, the inviscid and turbulent mass flux quantitities at any station differ by a constant, at most.*

This constant is readily determined by evaluating the two mass flux quantities at $x = x_i$, where $Y_{L_f}^{m+1}$ and $(\rho_f/\rho_\infty)\, Y_{T_f}^{m+1}$ are both

---

*Near the neck (dy_f/dx) and β_f may be comparable, and some error could be introduced by neglecting the interaction effect. However, the wake flow is "pressure-controlled" in the first 5 - 10 body diameters downstream of the neck in any case. Beyond $x/d \cong 10$, $\beta_f \ll (dy_f/dx)$.

$\lesssim 1$. When $z_f \ll 1$, $1 + H = \left(h_L/h_{\infty}\right)_0 \cong \left(h_f/h_{\infty}\right)$, and according to Eq. (37d),

$$p_f/p_{\infty}\left(\tilde{\gamma}_f\right)^{m+1} = \left(Y_{L_f}\right)^{m+1}\left(1+H\right) \tag{A.2-2}$$

or

$$\rho_f/\rho_{\infty}\left(\tilde{\gamma}_f\right)^{m+1} \cong \left(Y_{L_f}\right)^{m+1} \tag{A.2-3}$$

By inverting Eq. (4), taking $\rho_f/\rho = h/h_f$, and utilizing Eq. (3), one finds on the other hand that

$$\left(\tilde{\gamma}_f\right)^{m+1} \cong Y_{T_f}{}^{m+1} + \frac{(m+1)\,B_1 G_{m+1}\, Y_{T_f}{}^{m+1}}{H+1} \tag{A.2-4}$$

By employing Eq. (19), we have

$$\left(\rho_f/\rho_{\infty}\right)\tilde{\gamma}_f{}^{m+1} \cong \left(\rho_f/\rho_{\infty}\right) Y_{T_f}{}^{m+1} + (m+1)\,\frac{(\gamma_{\infty}-1)\,M_{\infty}^2}{(H+1)}\;\frac{(C_{D_f})_i}{4^{m+1}} \tag{A.2-5}$$

and by equating the two relations Eqs. (A.2-3) and (A.2-5) for $\tilde{\gamma}_f$, one obtains

$$Y_{L_f}{}^{m+1} - \left(\rho_f/\rho_{\infty}\right) Y_{T_f}{}^{m+1} = \delta = \frac{(m+1)}{4^{m+1}}\;\frac{(\gamma_{\infty}-1)\,M_{\infty}^2}{(1+H)}\,(C_{D_f})_i \tag{A.2-6}$$

or

$$\left(\rho_f/\rho_{\infty}\right)\alpha_m{}^{m+1}\, Y_{T_f}{}^{m+1} = z_f{}^{m+1} - \alpha_m{}^{m+1}\,\delta \tag{A.2-7}$$

where (Eqs. (A.1-9) and (A.2-6))

$$\alpha_m{}^{m+1}\,\delta = (m+1)\,g_{m+1}\;\frac{H}{H+1}\;\frac{(C_{D_f})_i}{C_{D_0}}\,. \tag{A.2-8}$$

APPENDIX 3

SOME REMARKS ON TOWNSEND'S EXPERIMENTAL RESULTS FOR LOW-SPEED WAKES: RELATION BETWEEN OUR K AND TOWNSEND'S R_T

According to Townsend's experimental results[6] $\tau = \rho \epsilon_T (\partial u/\partial y)$ near the axis of a symmetrical low-speed wake behind a long cylindrical rod normal to a uniform air stream, where ϵ_T is independent of y. Once the wake flow becomes "self-preserving" the mean velocity distribution near the wake axis is described by the parabola

$$\frac{u_f - u}{u_f - u(0)} \cong 1 - a(y^2/y_f^2) \qquad \text{(A.3-1)}$$

where a is a constant. Thus

$$\tau = -2a\rho\epsilon_T \left(\Delta u \frac{y}{y_f^2}\right) \qquad \text{(A.3-2)}$$

where $\Delta u = u_f - u(0)$. But $\tau = -\rho\overline{u'v'}$, and the question arises as to whether Eq. (A.3-2) for τ is consistent with the behavior of the correlation $\overline{u'v'}$ across the wake.

Townsend[6] found that the turbulent velocity fluctuations require a somewhat longer distance behind the rod to reach equilibrium, or "similarity", than the mean axial velocity. Nevertheless this similarity is well established at x/d = 500 (Figures 7.1 and 7.4, p. 135 and pp. 142-143, Reference 6). In Section 2.1 it was pointed out that the characteristic length in our case is not the body diameter but the inner wake momentum thickness, θ. Therefore on the basis of Townsend's

results and our estimates of θ_i/d, one should expect complete flow similarity in the inner wake to be established in 5 - 20 body diameters. Once this similarity exists

$$\frac{-\overline{u'v'}}{u'^2} = g(y/y_f) \qquad \text{(A.3-3)}$$

and by symmetry

$$g(y/y_f) \sim y/y_f \qquad \text{(A.3-3a)}$$

near the wake axis (Figure 7.10, page 152, Reference 6). The quantity $\overline{u'^2}$ is virtually independent of y near the wake axis and its magnitude decays with downstream distance exactly like $(\Delta u)^2$ (Figure 7.4, page 142, Reference 6). In other words $\overline{u'^2} \sim (\Delta u)^2$. By combining this statement with Eq. (A. 3-3) and (A. 3-3a), we find that

$$\tau = -\rho\,\overline{u'v'} \sim -\rho(\Delta u)^2(y/y_f) \qquad \text{(A.3-4)}$$

Clearly Eq. (A.3-2) and (A.3-4) for τ are compatible if $\epsilon_T \sim \Delta u\, y_f$, or if the quantity $\frac{\Delta u\, y_f}{\epsilon_T}$ is a universal constant "Reynolds number" for the symmetrical wake flow. In this particular case, the validity of the semi-empirical relation $\tau = \rho\epsilon_T(\partial u/\partial y)$ is assured by symmetry and similarity; in fact one could dispense with it entirely and work directly with the Reynolds stress. Evidently these same arguments are applicable to axially-symmetric "similar wakes", and by Reynolds' analogy, to the turbulent transfer of mass and heat.

The only remaining question is the magnitude of the Reynolds number $\frac{\Delta u\, y_f}{\epsilon_T}$, which must be determined by rough physical arguments about the

characteristic size and shape of the large eddies[6], or by experiment[6]. The procedure adopted here is to make certain that the relation between the turbulent diffusivity and the drag coefficient of the wake (Eq. (18a)) reduces to Townsend's relation for isothermal flow. In this way our K is related directly to Townsend's

$$R_T = \frac{\Delta u \, l_o}{\epsilon_T} \tag{A.3-5}$$

where l_o is a measure of the wake width. In Townsend's case, the mean axial velocity distribution not too near the edge of the wake is described very closely by the Gaussian distribution

$$\frac{u_\infty - u}{u_\infty - u(0)} = \exp\left\{-\frac{y^2}{2 l_o^2}\right\} \tag{A.3-6}$$

Thus (Eq. (14))

$$C_{D_f} = 4^{m+1}\left(\Delta u / u_\infty\right) 2^{\frac{m+1}{2}} \left(l_o/d\right)^{m+1} F_{m+1} \tag{A.3-7}$$

where $F_1 = \sqrt{\pi/2}$ and $F_2 = \frac{1}{2}$. By using Eq. (A.3-5) and (A.3-7), we have

$$\left(\epsilon_T/u_\infty d\right)\left(l_o/\quad\right)^{m} = \left(R_T\right)^{-1} \frac{C_{D_f}}{4^{m+1}} \quad \frac{1}{2^{\frac{m+1}{2}} F_{m+1}} \tag{A.3-8}$$

Now for isothermal wakes of Townsend's type our Eq. (18a) for $\tilde{\epsilon}_T$ (or ϵ_T) reduces to the form

$$\frac{\epsilon_T}{u_\infty d}\left(Y_{T_f}\right)^{m} \cong \frac{K}{4^{m+1} G_{T_{m+1}}} C_{D_f} \tag{A.3-9}$$

By equating Eq. (A. 3-8) and (A. 3-9) for ϵ_T, one finds that

$$K = \frac{G_{m+1}}{2^{\frac{m+1}{2}} F_{m+1}} \left[\frac{Y_{T_f}}{(\ell_o/d)} \right]^m (R_T)^{-1} \qquad \text{(A.3-10)}$$

For a two-dimensional wake with a parabolic mean enthalpy profile, $G_1 = 2/3$, and

$$K = 0.53\ (R_T)^{-1} \qquad \text{(A.3-10a)}$$

or, taking Townsend's value of $R_T = 12.5$,

$$K = 0.043 \quad . \qquad \text{(A.3-10b)}$$

In the case of an axially-symmetric wake, the value of K depends to some extent on the "matching" between the velocity profile selected for the inner wake in our case and the Gaussian velocity profile for a low-speed wake spreading into an irrotational flow. By comparison with the experimental results of Townsend[6], and Hall[9] and Hislop, the "best fit" for a parabolic velocity profile is obtained by taking $Y_{T_f} = 2(\ell_o/d)$. At this point $(u_\infty - u) \simeq 0.05\ \Delta u$ for the actual profile (Figure 7.4, Reference 6), and the turbulent intensities $\overline{u'^2}$, $\overline{v'^2}$, and $\overline{w'^2}$ are less than 10 per cent of their peak values.*

---

* The problem of selecting the "best fit" is somewhat similar to the problem of choosing the "thickness" of a boundary layer along a solid surface. One wants to include the bulk of the mean shear flow, but not too much of the "external" inviscid flow. Fortunately in the axially-symmetric case the wake width at a given downstream location

With this choice of Y_{T_f}, and with $G_2 = 1/4$, and $R_T = 14.5$

$$K = 0.035 \cong 0.04 \qquad \text{(A.3-10c)}$$

This value of K is utilized throughout the numerical computations (Section 4).

---

* ξ depends on $K^{1/3}$ (Section 3.1), or on $\left(\frac{Y_{T_f}}{(\ell_o/d)}\right)^{1/3}$. However, the downstream location for a given wake width varies inversely with K. It should be noted that the intermittency factor γ is about 0.4 at the point $Y_{T_f} = 2\ell_o$ (Figure 7.5, Reference 6), and a sensitive hot-wire anemometer measuring turbulent fluctuations might find a "wake width" as much as 50 per cent greater than the wake width for the mean flow quantities.

APPENDIX 4

MOMENTUM DEFECT IN THE INNER WAKE AND ORDINARY DRAG; ESTIMATE OF INITIAL DRAG COEFFICIENT, $(C_{D_f})_i$

According to Eq. (18) the effective turbulent diffusivity is determined by the momentum defect D_f in the inner wake measured with respect to the local flow in the outer wake at the turbulent front. But the usual aerodynamic drag D_∞ is measured with respect to the free-stream velocity, u_∞. These two quantities are connected by the relation

$$D_f = 2(\pi)^m \int_0^{y_f} \rho_T u_T (u_f - u_T) y^m dy = \tag{A.4-1}$$

$$= 2(\pi)^m \int_0^{y_f} \rho_T u_T (u_\infty - u_T) y^m dy - 2(\pi)^m \int_0^{y_f} \rho_T u_T (u_\infty - u_f) y^m dy$$

or,

$$D_f = D_\infty - \dot{m}_T (u_\infty - u_f) \tag{A.4-2}$$

where $\dot{m}_T$ is the mass flux in the turbulent inner wake. Even in the initial stages near the neck, where D_f is very nearly constant, D_∞ increases in the downstream direction because the inner wake is capturing additional mass flux, and the term $\dot{m}_T (u_\infty - u_f)$ takes account of the differences in momentum flux as measured in the two different coordinate systems.

Once the process of swallowing momentum defect begins D_f and D_∞ both vary along the wake axis. Of course the total momentum defect is constant when $(p - p_\infty) << \frac{1}{2}\rho_\infty u_\infty^2$, and so is the difference between the turbulent and inviscid drags of the inner wake for the same mass flux. This relation can be derived as follows:

According to Eq. (A.4-2) the difference ΔD_f can be written

$$\Delta D_f = 2(\pi)^m \left[\int_0^{y_f} \rho_T u_T (u_f - u_T) y^m dy - \int_0^{y_f} \rho_L u_L (u_f - u_1) y^m dy \right]$$

$$= 2(\pi)^m \left[\int_0^{y_f} \rho_T u_T (u_\infty - u_T) y^m dy - \int_0^{y_f} \rho_L u_L (u_\infty - u_L) y^m dy \right] \qquad (A.4\text{-}3)$$

Now

$$D_{TOTAL} = 2(\pi)^m \left[\int_0^{y_f} \rho_T u_T (u_\infty - u_T) y^m dy + \int_{y_f}^{\infty} \rho_L u_L (u_\infty - u_L) y^m dy \right] = \text{const.} \qquad (A.4\text{-}4)$$

or

$$D_{TOTAL} = 2(\pi)^m \left[\int_0^{\infty} \rho_L u_L (u_\infty - u_L) y^m dy + \left\{ \int_0^{y_f} \rho_T u_T (u_\infty - u_T) y^m dy - \int_0^{y_f} \rho_L u_L (u_\infty - u_L) y^m dy \right\} \right] = \text{const.} \qquad (A.4\text{-}5)$$

The first integral in Eq. (A.4-5) represents the drag D_o of the original flow in the outer wake, and is a constant; therefore the quantity in $\{\ \}$, which is identical with ΔD_f, is also a constant. The constant is determined by evaluating ΔD_f when $\tilde{y}_f << 1$. In that case $u_L \tilde{=} u_f$,

and

$$\Delta D_f \cong 2(\pi)^m \int_0^{(y_f)_i} \rho_T u_T (u_{r_T} - u_T) y^m dy \quad ,$$

which is exactly the initial momentum defect of the inner wake with respect to the local flow in the outer wake at the front. The fact that ΔD_f is constant can also be verified by utilizing Eq. (20).; the rate of increase of the first term in Eq. (A.4-3), which determines the turbulent diffusivity, is exactly balanced by the rate of increase of the second term.

A precise value of $(D_f)_i$ or $(C_{D_f i})$ is difficult to determine at present, but a rough estimate is obtained by equating $(D_f)_i$ to the sum of the skin friction drag on the body and the additional momentum defect produced by the pressure rise at the neck (Figure 1). According to the momentum equation, this increase in momentum defect is given by

$$\Delta\left[2(\pi)^m \int_0^{y_f} \rho u (u_{r_T} - u) y^m dy\right] \cong \frac{2(\pi)^m (y_f)_i^{m+1}}{m+1} \Delta p \qquad \text{(A.4-6)}$$

where Δp is the pressure rise at the neck. Viscous stresses are neglected because the compression occurs over a short distance[4]. Let the subscripts 1 and 2 denote conditions just upstream and downstream of the neck, respectively. Then $\Delta p = p_1\left(\frac{p_2}{p_1} - 1\right)$ and (Eq. (A.4-6))

$$\Delta C_{D_f} \cong 2^{m+1}\left(\frac{2}{\gamma_\infty M_\infty^2}\right)\left(\frac{p_1}{p_\infty}\right)\left(\frac{p_2}{p_1}-1\right)\left(\frac{y_f}{d}\right)^{m+1} \qquad \text{(A.4-7)}$$

For two-dimensional flow the quantities p_2 and p_1/p_∞ can be evaluated approximately. C. F. Dewey, Jr.* points out that for an isentropic compression process p_2 is equal to the pressure on the body surface at the point where the streamline is parallel to the free stream direction. By employing a Prandtl-Meyer expansion from the sonic point on a blunt-nosed body this pressure is evaluated, and by using Chapman's criterion for p_2/p_1, Dewey finds that $p_1/p_\infty \cong 1.3 \times 10^{-2}\ (\gamma_\infty M_\infty^2)$. Also $p_2/p_1 \cong 3$ because $M_1 \cong 3$, virtually independent of M_∞.

The remaining unknown is the neck width $(y_f/d)_i$. This width is determined by the boundary layer thickness at the separation point on the body surface, plus the subsequent mass flux entrainment in the free shear layer. A rough estimate of $(y_f/d)_i$ for the case of a circular cylinder is obtained by considering this whole process to be equivalent to the development of the laminar boundary layer over a blunt-nosed slab of equivalent length. Since the free shear layer makes an angle of about 17° with the free stream direction the neck location corresponds approximately to $\Delta/d = 2.3$. Calculations similar to those made in Reference 22 for a hemisphere-cylinder yield $(\delta^*/d)_i \sqrt{Re_d} \cong 18$, or $\left(\frac{\delta}{d}\right)_i \sqrt{Re_d} = \left(\frac{y_f}{d}\right)\sqrt{Re_d} \cong$ **.

---

* Private communication.

** The boundary layer in the two-dimensional case is thicker than it is on the hemisphere-cylinder by the factor $\sqrt{2}$.

This rough estimate is in fair agreement with measurements of the neck width in the wake behind a circular cylinder made by C. F. Dewey, Jr.,[23] at $M_\infty = 5.8$.

In the axially-symmetric case the inviscid flow is more complicated near the neck. For the present, we utilize the estimates for p_1/p_∞ and p_2/p_1 obtained from two-dimensional flow considerations. If the ratio of mass flux in the inner layer at the neck to the mass flux at the boundary layer separation point is the same as in the two-dimensional case, then mass continuity dictates that the quantity $(y_f/d)_i^2$ must be equal to the two-dimensional value of $(y_f/d)_i$, divided by the factor $\sqrt{2}$.

Collecting all of these estimates we find that

$$\Delta C_{D_f} \cong 2^{m/2} \frac{3.7}{\sqrt{Re_d}} \qquad \text{(A.4-8)}$$

Now $C_{D_{f_i}} = C_f + \Delta C_{D_f}$, where C_f is the skin-friction drag coefficient of the body. Roughly $C_f \cong \frac{(1.3)\,2^{m/2}}{\sqrt{Re_d}}$,
so that

$$(C_{D_f})_i \cong 2^{m/2} \cdot \frac{5}{\sqrt{Re_d}} \qquad \text{(A.4-9)}$$

Since the probable minimum Reynolds number for turbulent flow in the wake[3] is of the order of 5×10^4, the maximum relevant value of $(C_{D_f})_i$

is about 0.02 in the two-dimensional case, and about 0.028 in the axially-symmetric case. This condition corresponds to a flight altitude of about 180,000 feet for a body one foot in diameter at satellite velocity. At an altitude of 100,000 feet, for example, $Re_d \tilde{=} 2.5 \times 10^6$ for the same body, so that $(C_{D_f})_i \tilde{=} 0.0033$ in the two-dimensional case and $(C_{D_f})_i \tilde{=} 0.005$ in the axially-symmetric case. In the numerical examples of Section 4 the value of 0.022 for $(C_{D_f})_i$ at $M_\infty = 8.5$ corresponds to a Reynolds number near the lower limit, while the value 0.0077 for $M_\infty = 22$ corresponds to $Re_d \tilde{=} 8 \times 10^5$.

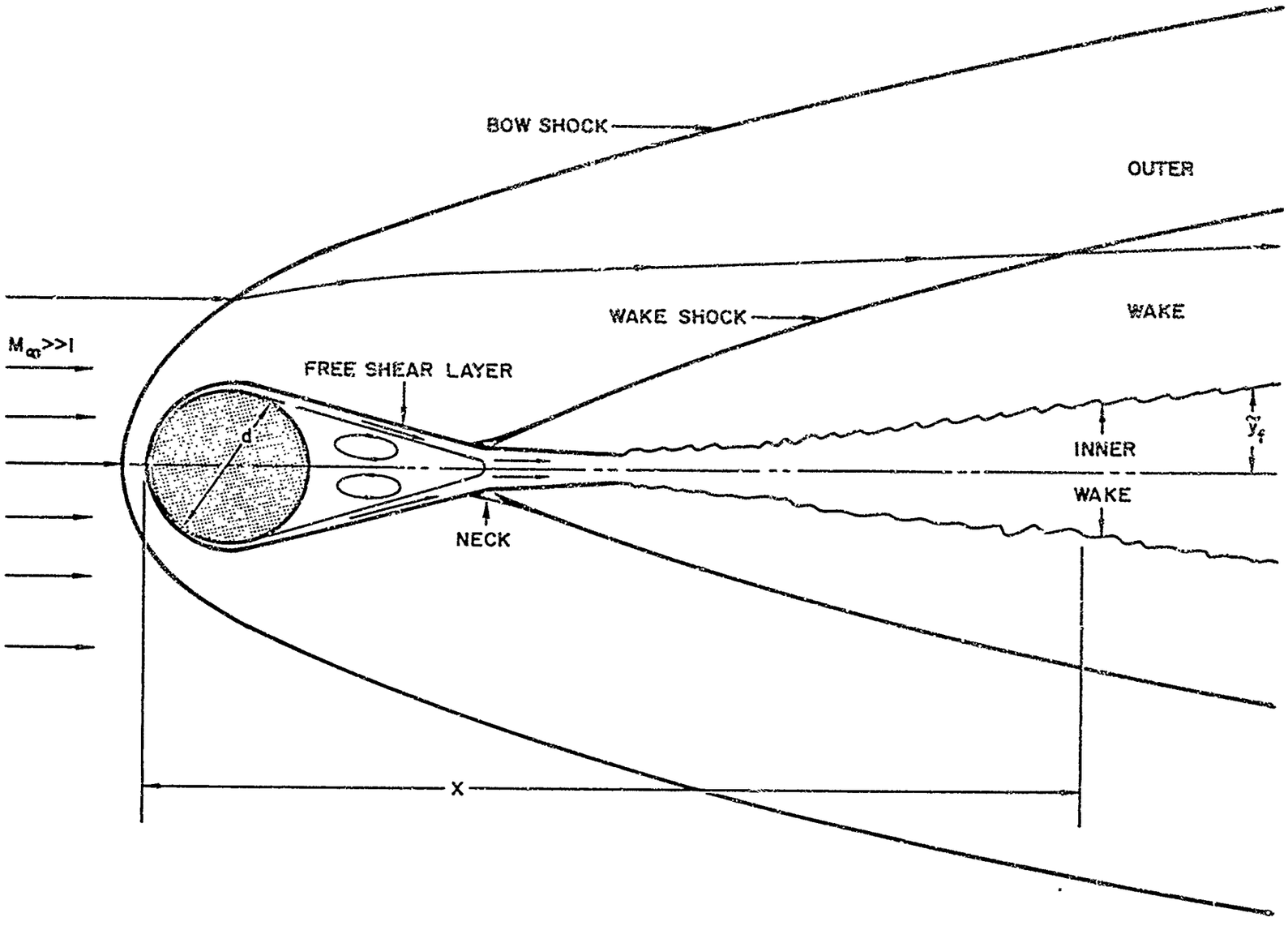

Figure 1. Wake Behind Blunt Body at Hypersonic Speeds

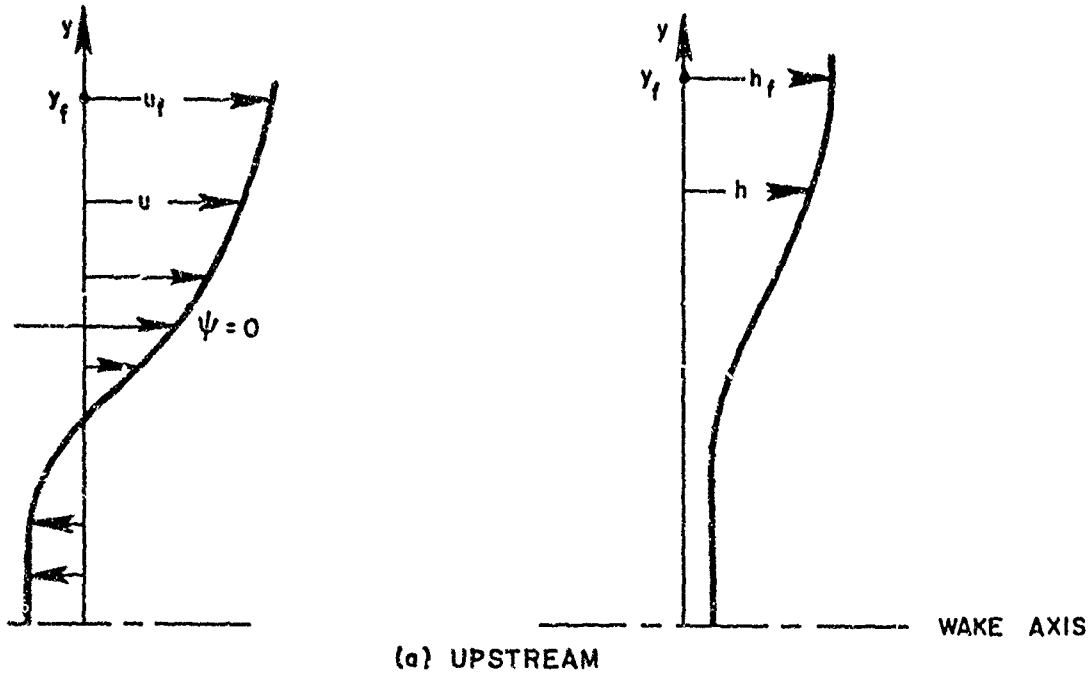

Figure 2. Typical Inner Wake Velocity and Enthalpy Profiles just Upstream and Downstream of Neck

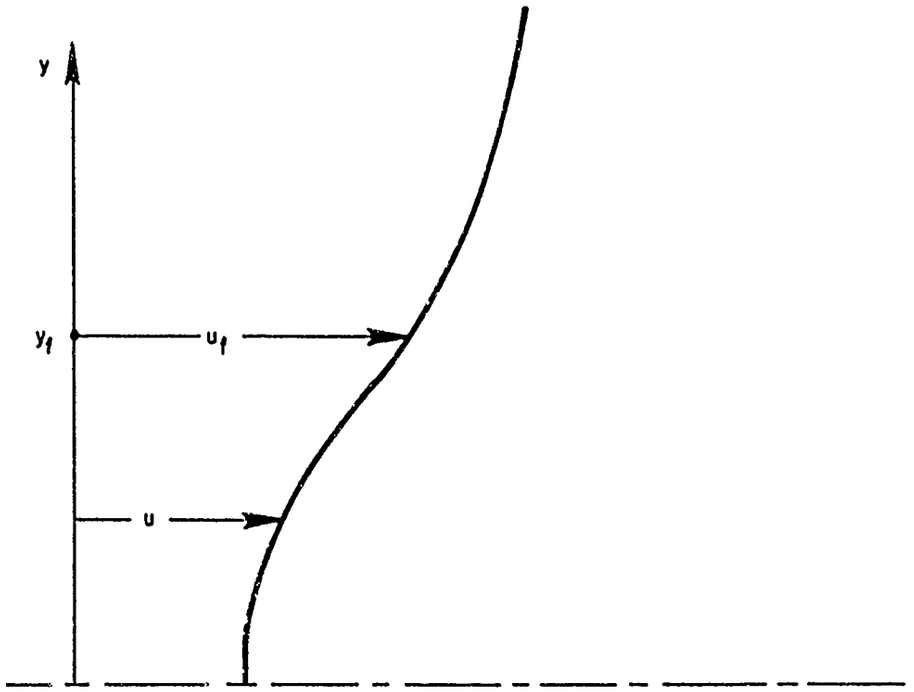

(3a)

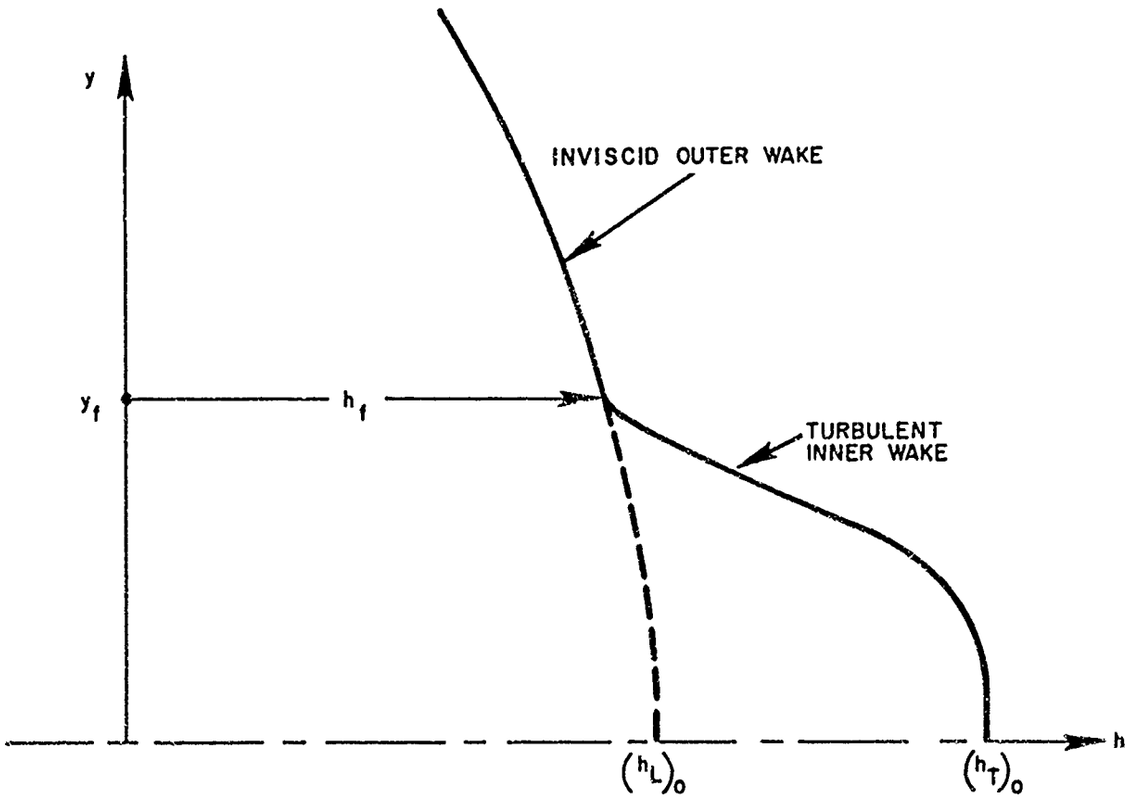

(3b)

Figure 3. Typical Velocity and Enthalpy Profiles at x/d $\cong$ 10

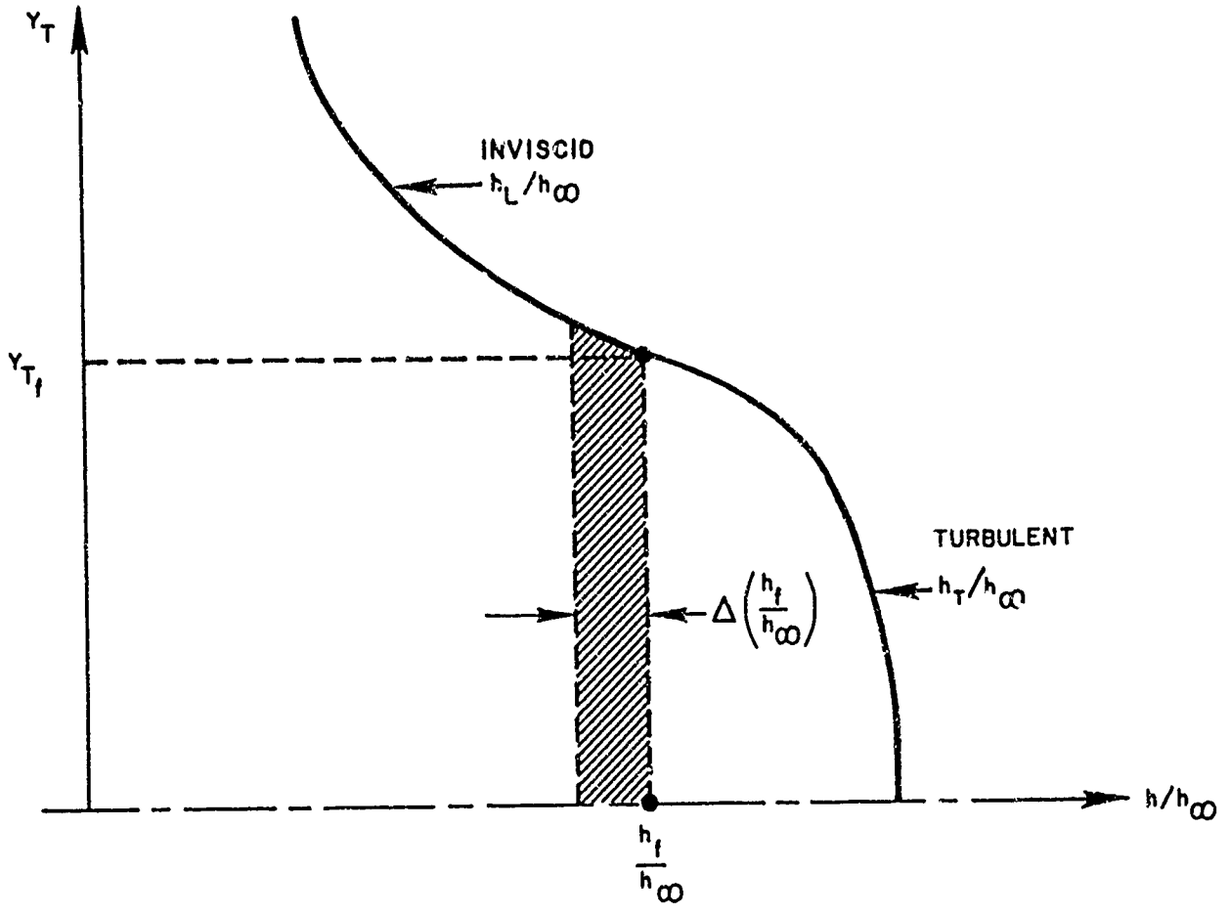

Figure 4. Swallowing of Enthalpy Excess or Momentum Defect by Inner Wake

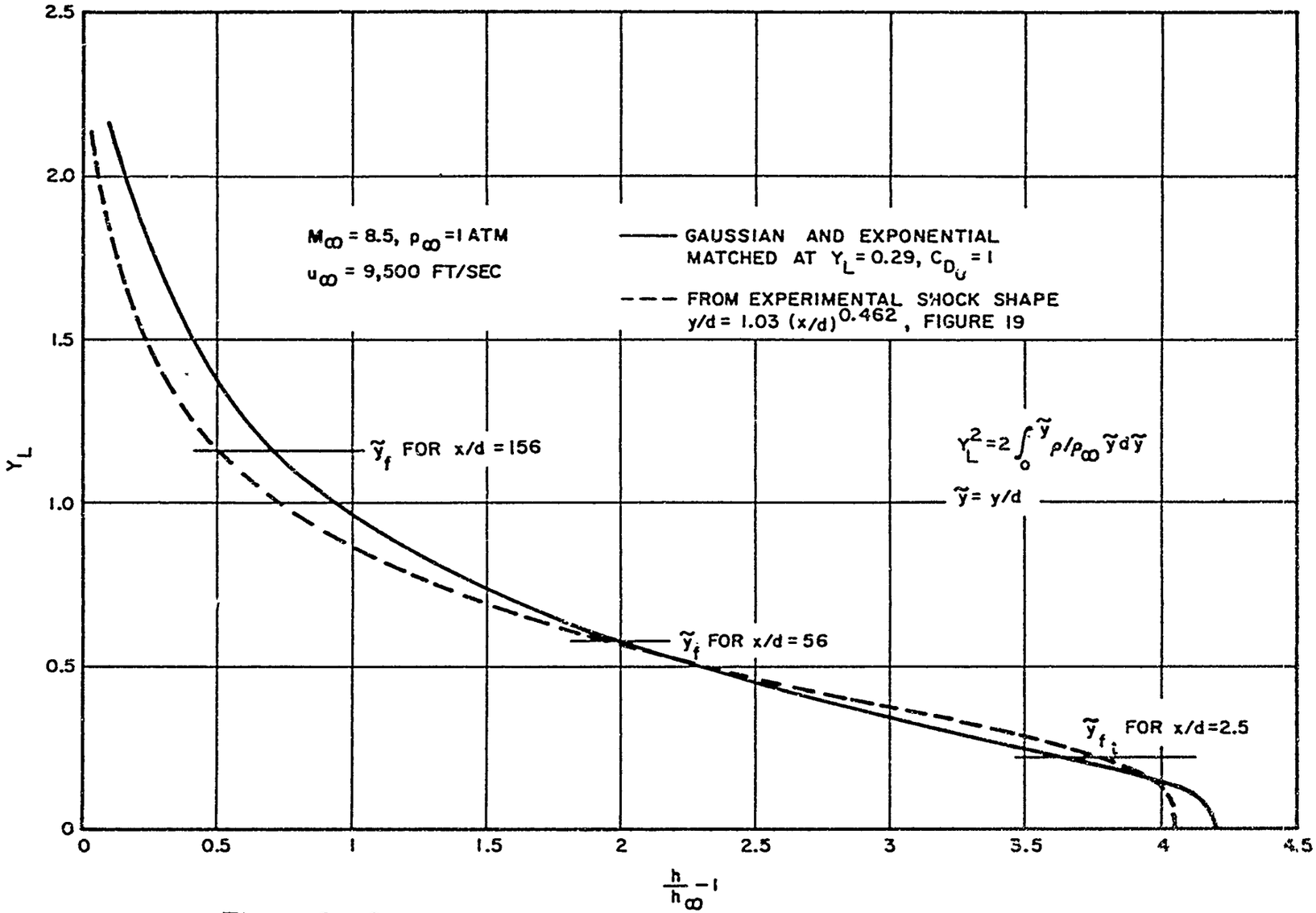

Figure 5. Outer Inviscid Enthalpy Profile (M_∞ = 8.5 and p_∞ = 1 ATM)

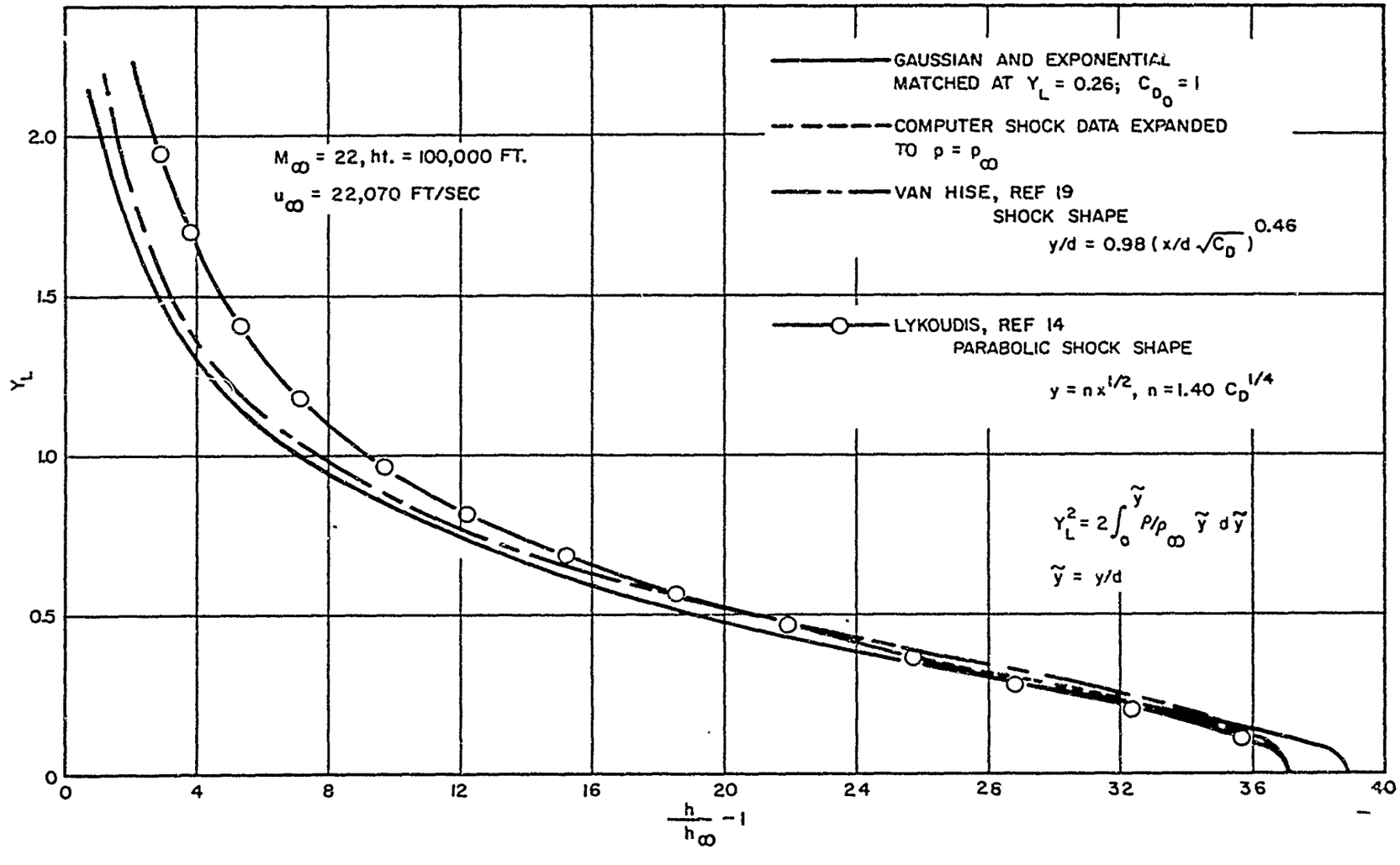

Figure 6. Outer Inviscid Enthalpy Profile (M_∞ = 22 and 100,000 ft Altitude)

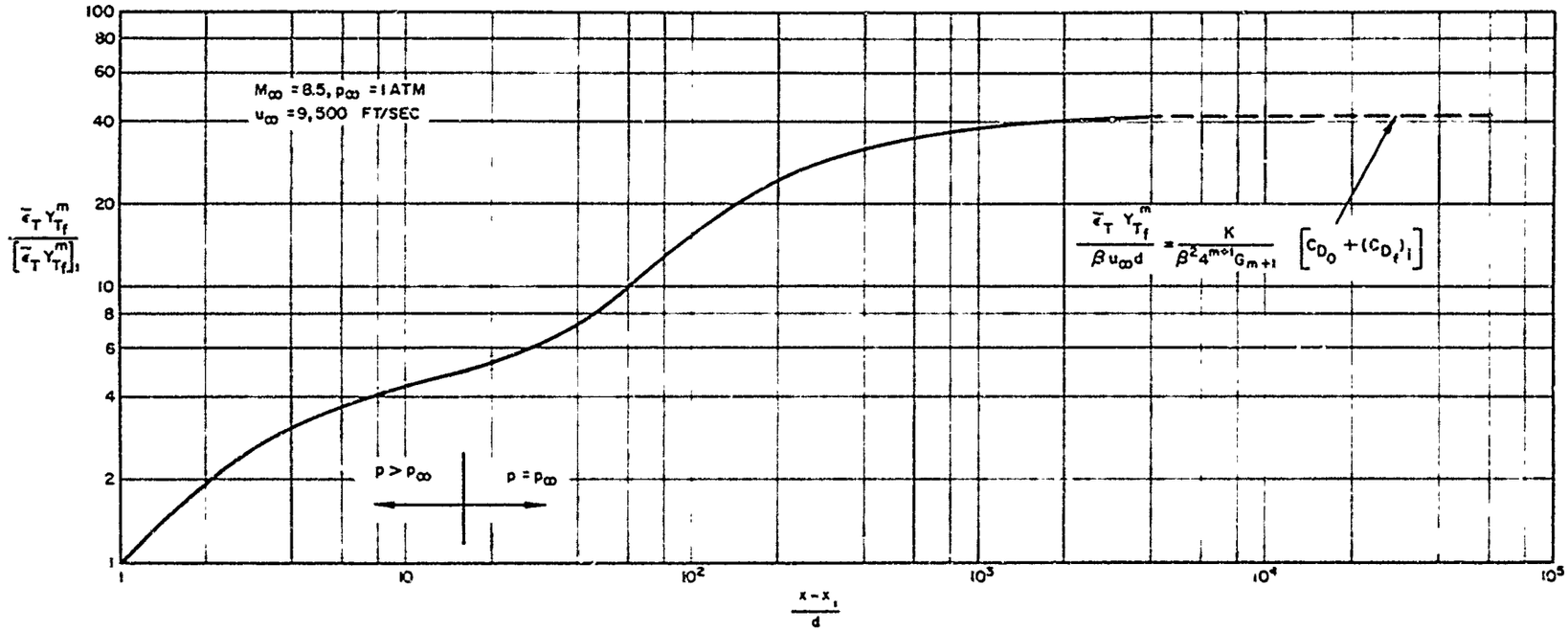

Figure 7. Growth of the Turbulent Diffusivity ($M_\infty = 8.5$ and $p_\infty = 1$ ATM)

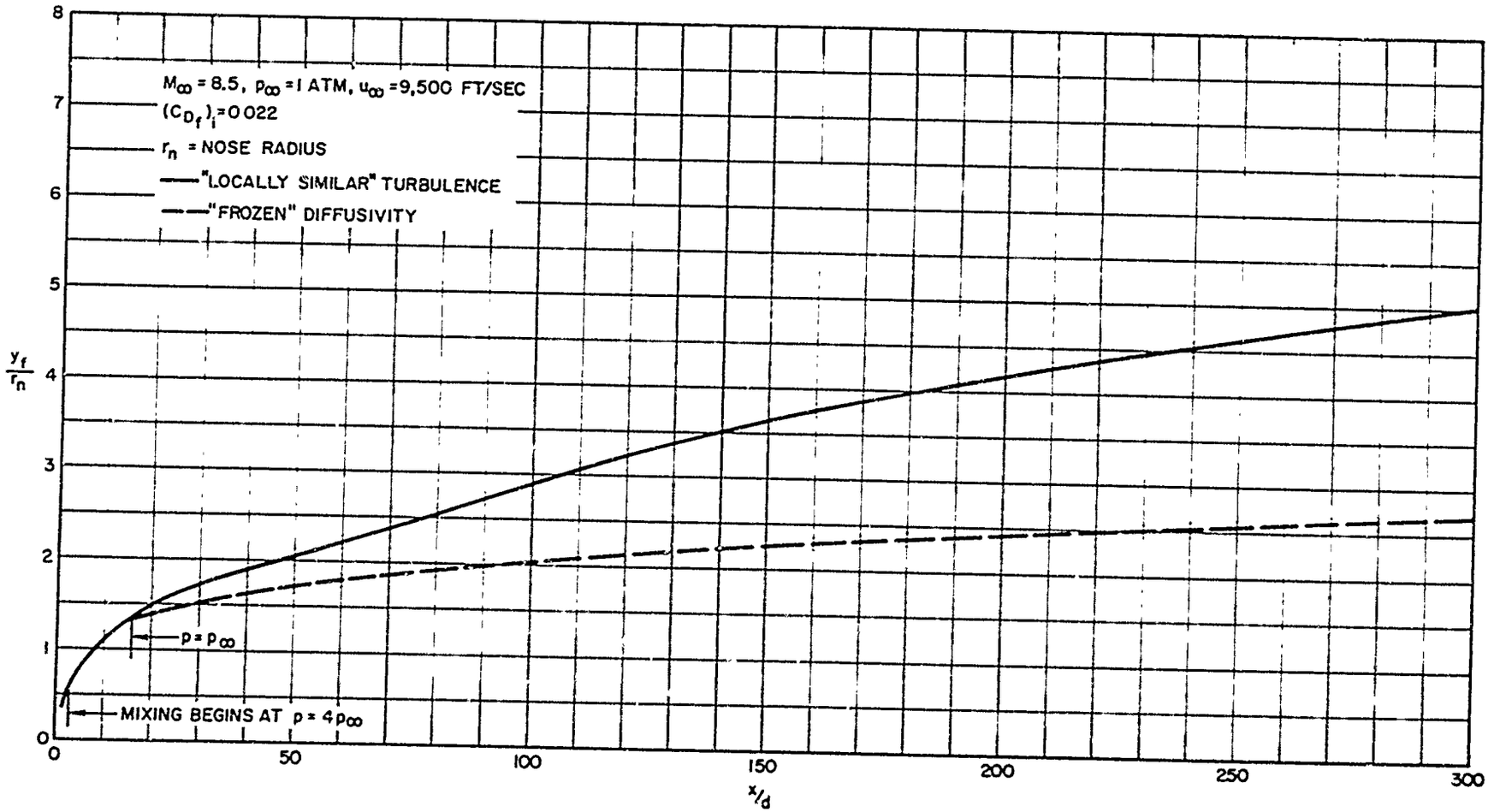

Figure 8. Turbulent Wake Width (M_∞ = 8.5 and p_∞ = 1 ATM)

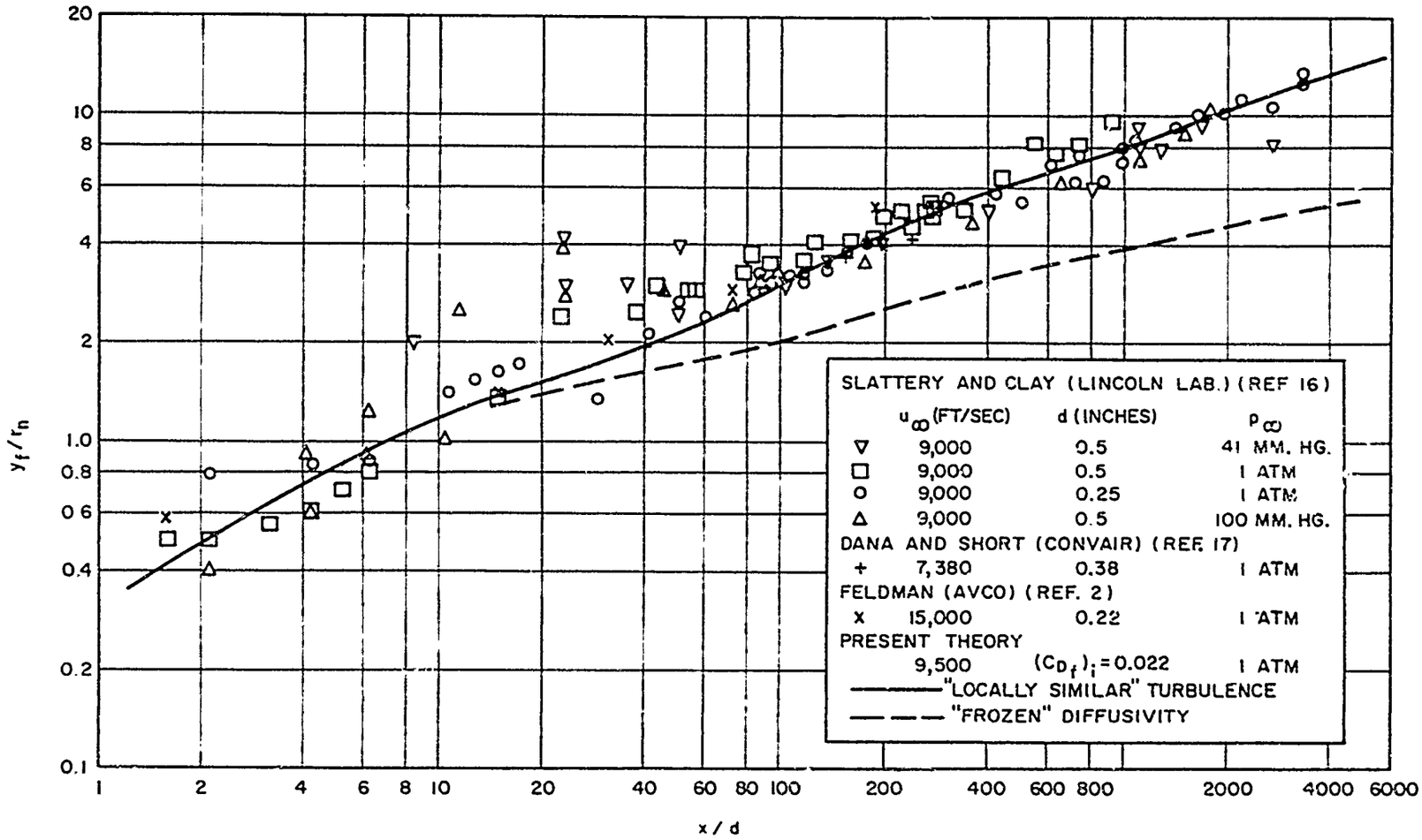

Figure 9 Comparison of Theory and Experiment for Turbulent Wake Width (M_∞ 8.5 and p_∞ = 1 ATM)

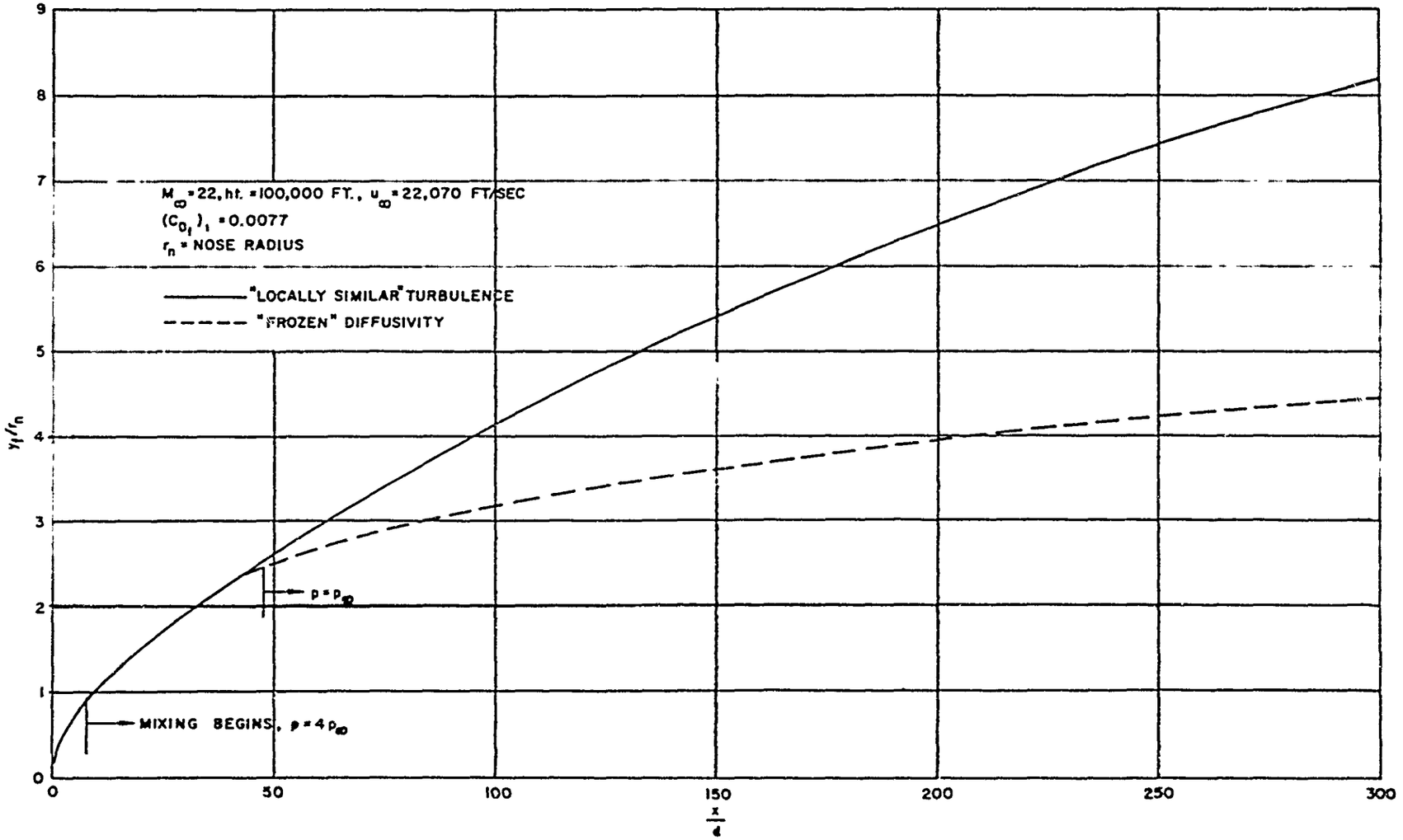

Figure 10. Turbulent Wake Width (M_∞ = 22 and 100,000 ft Altitude)

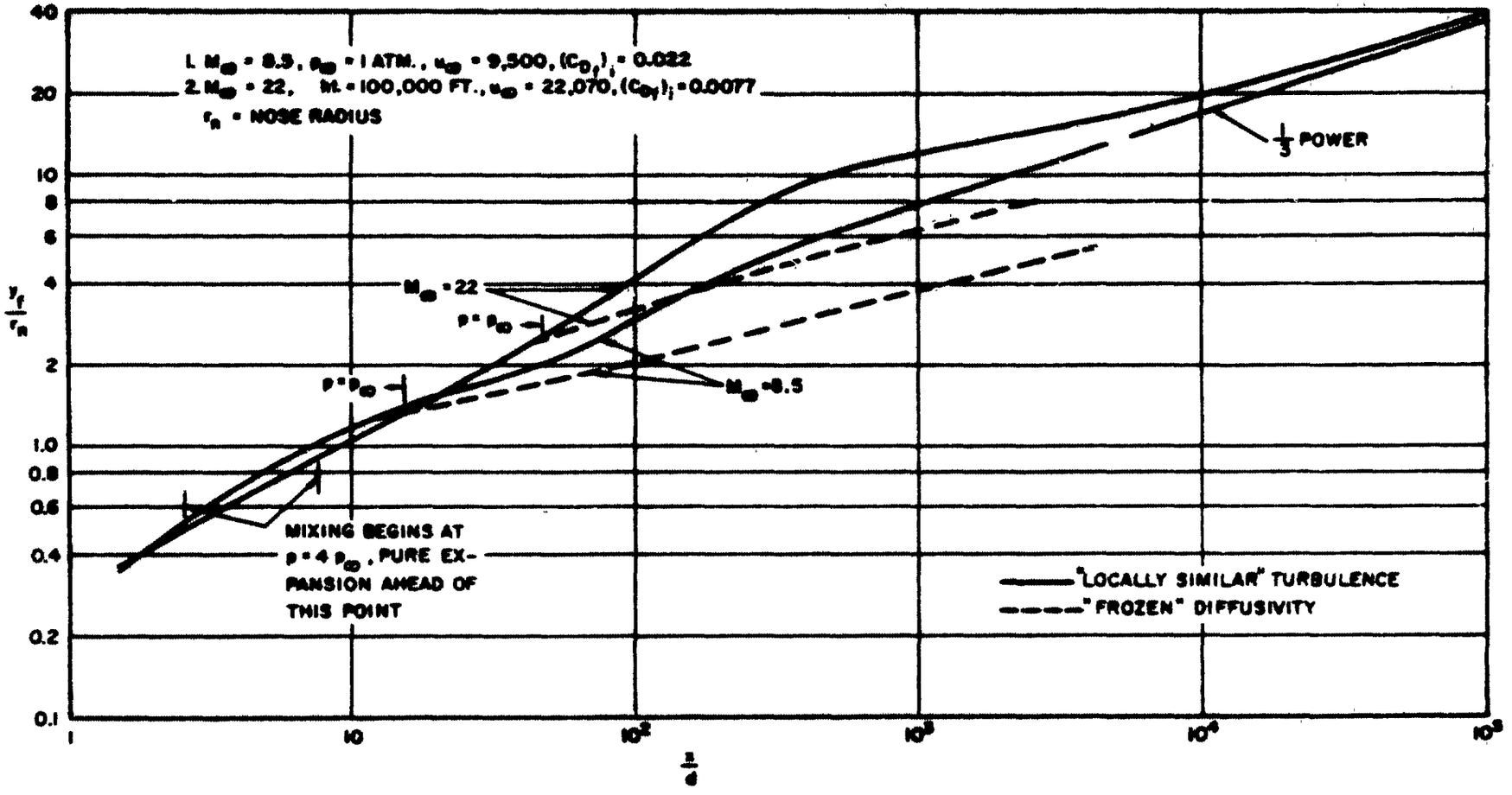

Figure 11. Comparison of Turbulent Wake Width for M_∞ = 8.5 and M_∞ = 22

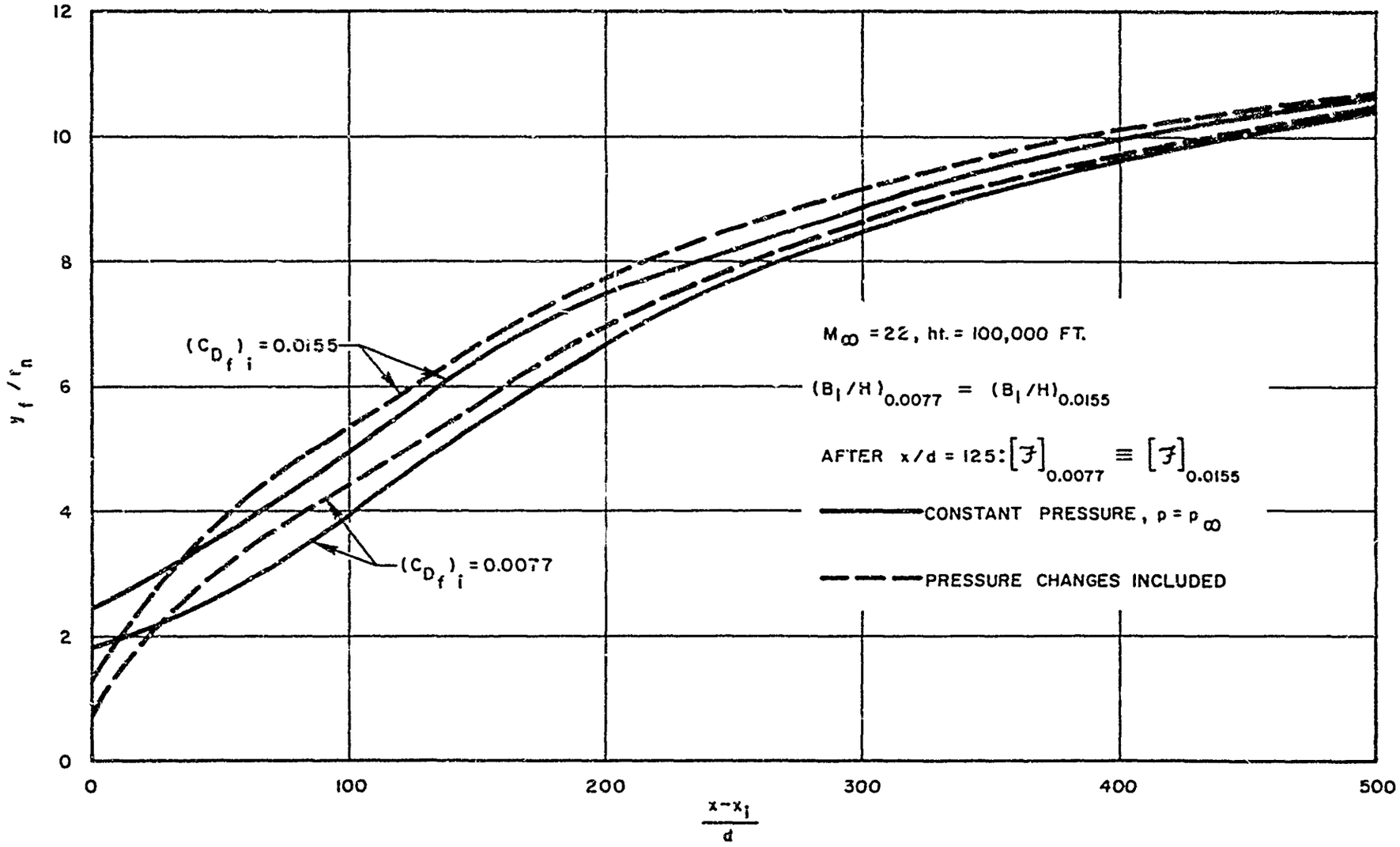

Figure 12. Effect of Initial Turbulent Drag Coefficient on Wake Growth

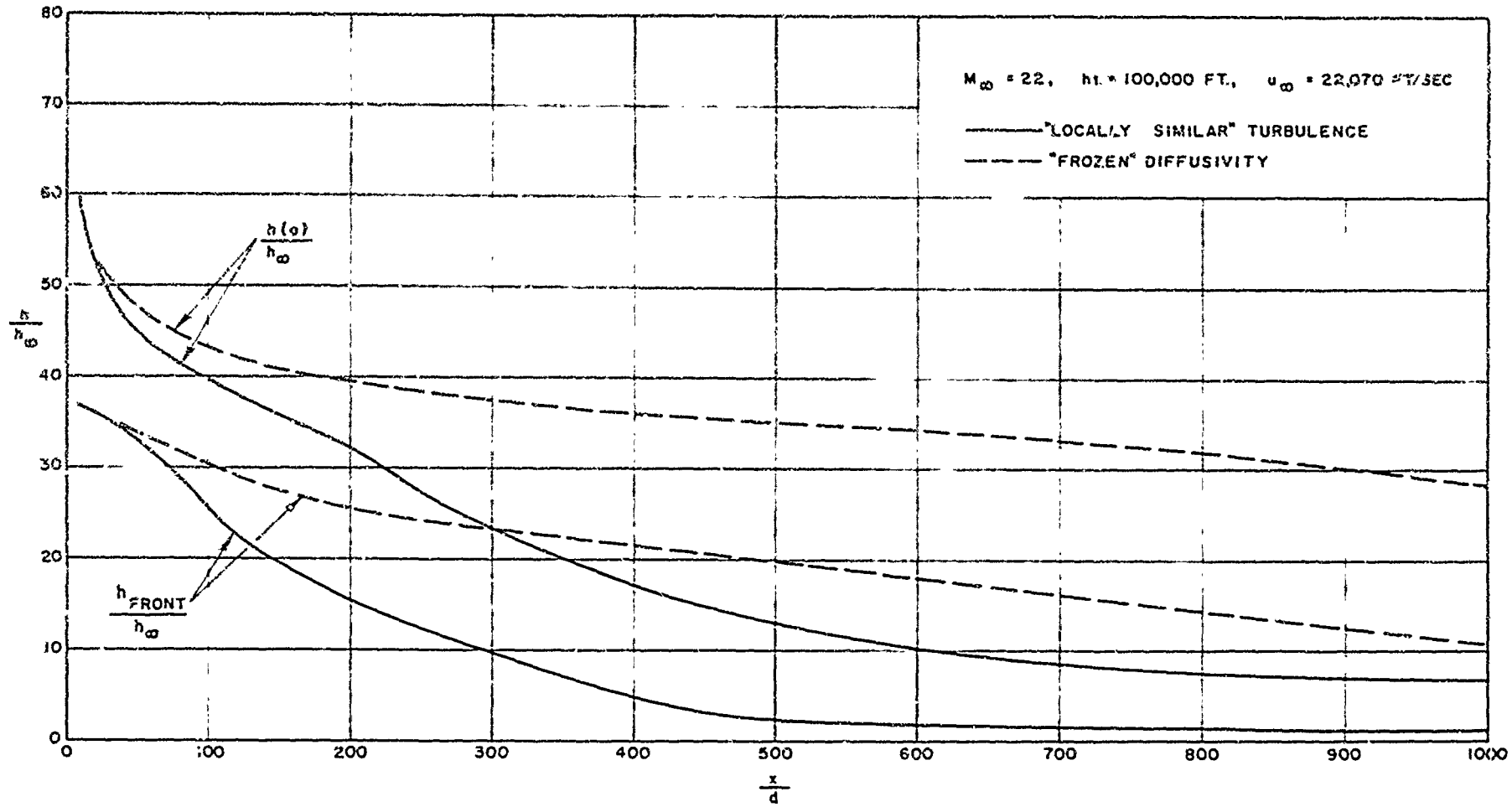

Figure 13. Enthalpy Distribution Along the Axial Streamline (M_∞ = 22 and 100,000 ft Altitude)

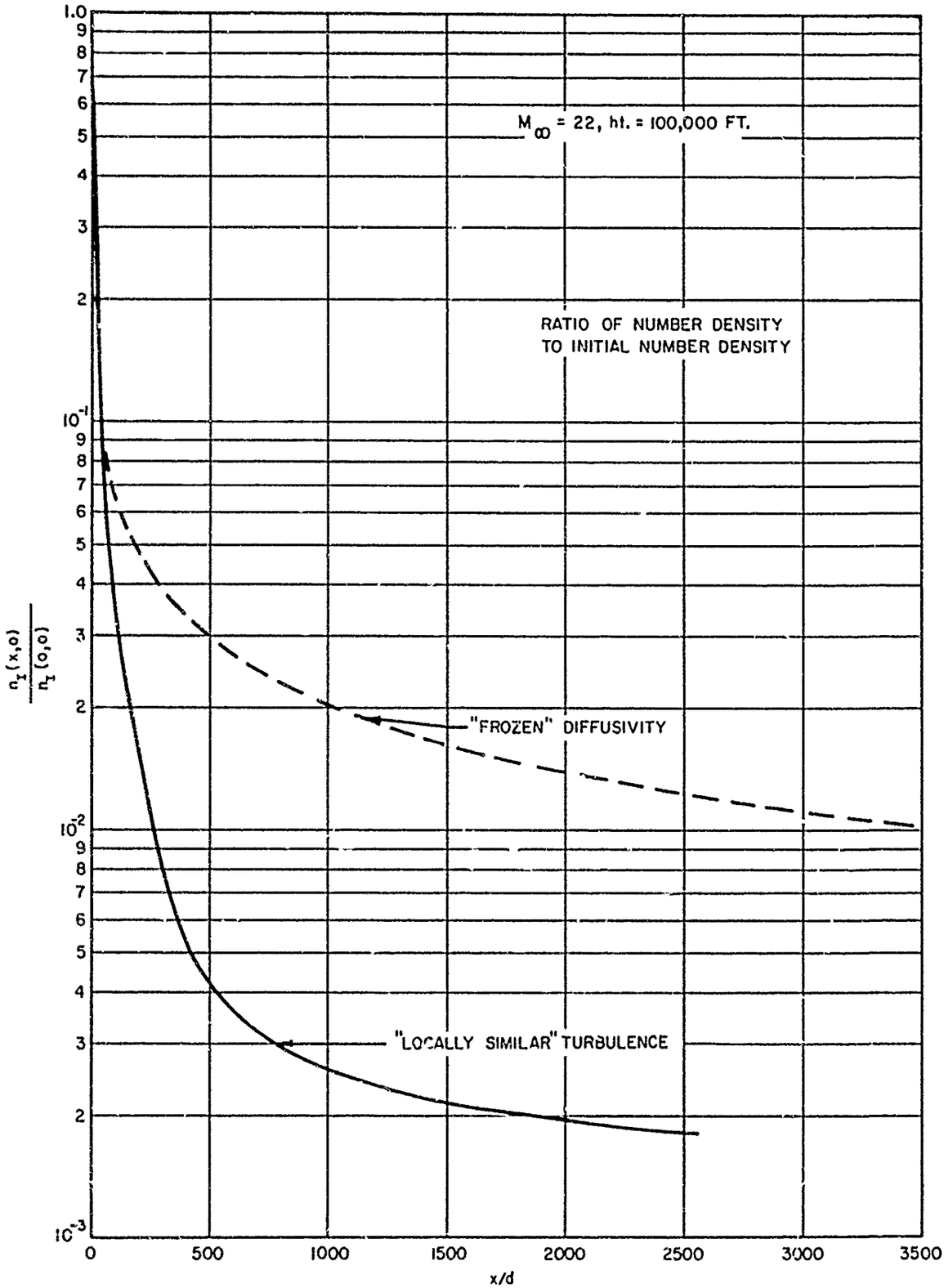

Figure 14. Turbulent Diffusion in the Wake
(M_∞ = 22 and 100,000 ft Altitude)

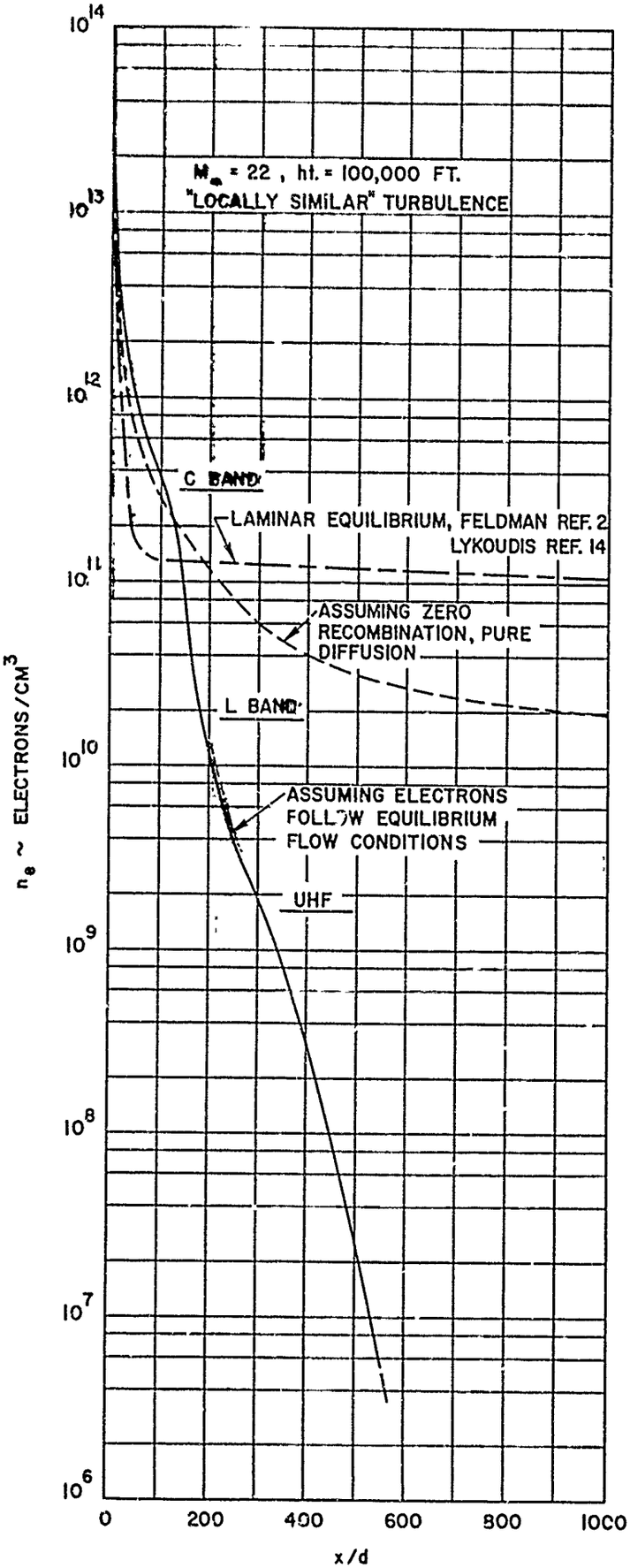

Figure 15. Electron Densities Along the Axial Streamline (M_∞ = 22 and 100,000 ft Altitude)

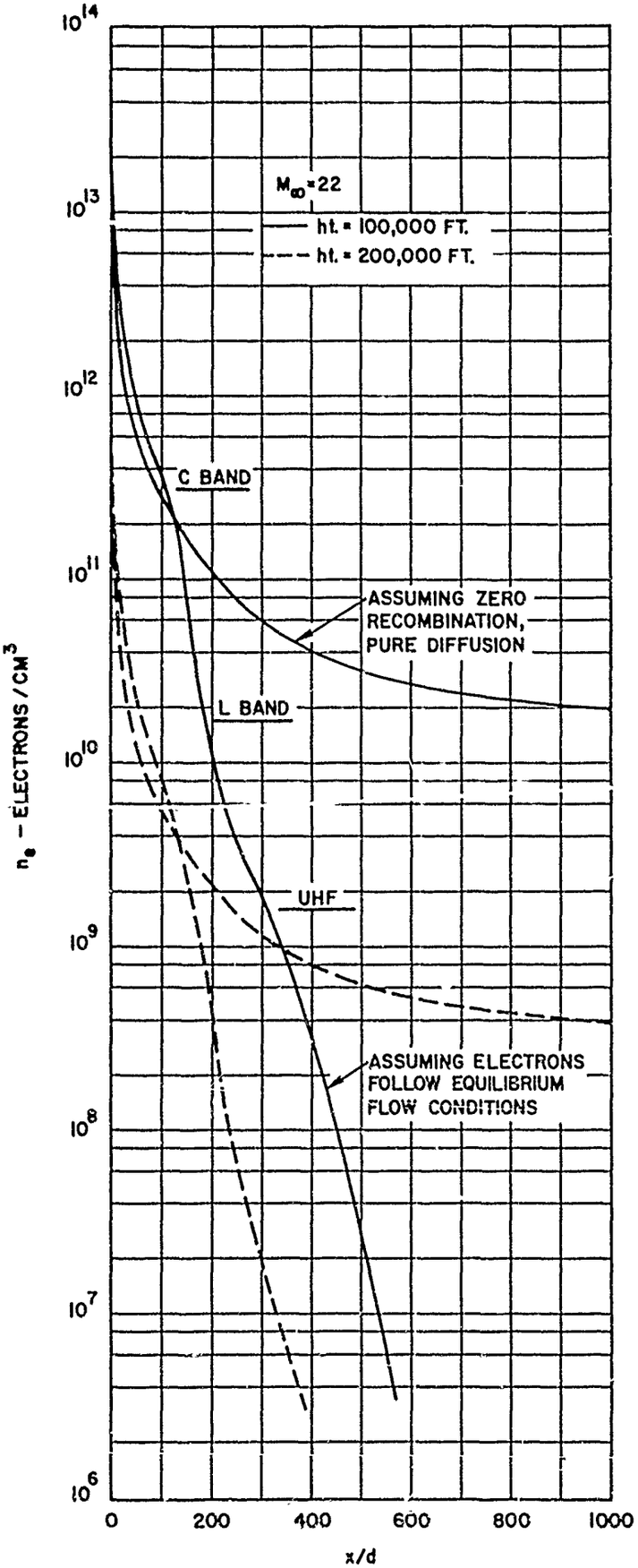

Figure 16. Electron Densities Along the Axial Streamline (M_∞ = 22, 100,000 and 200,000 ft Altitudes)

Figure 17. Radial Electron Density Distributions (M_∞ = 22 and 100,000 ft Altitude)

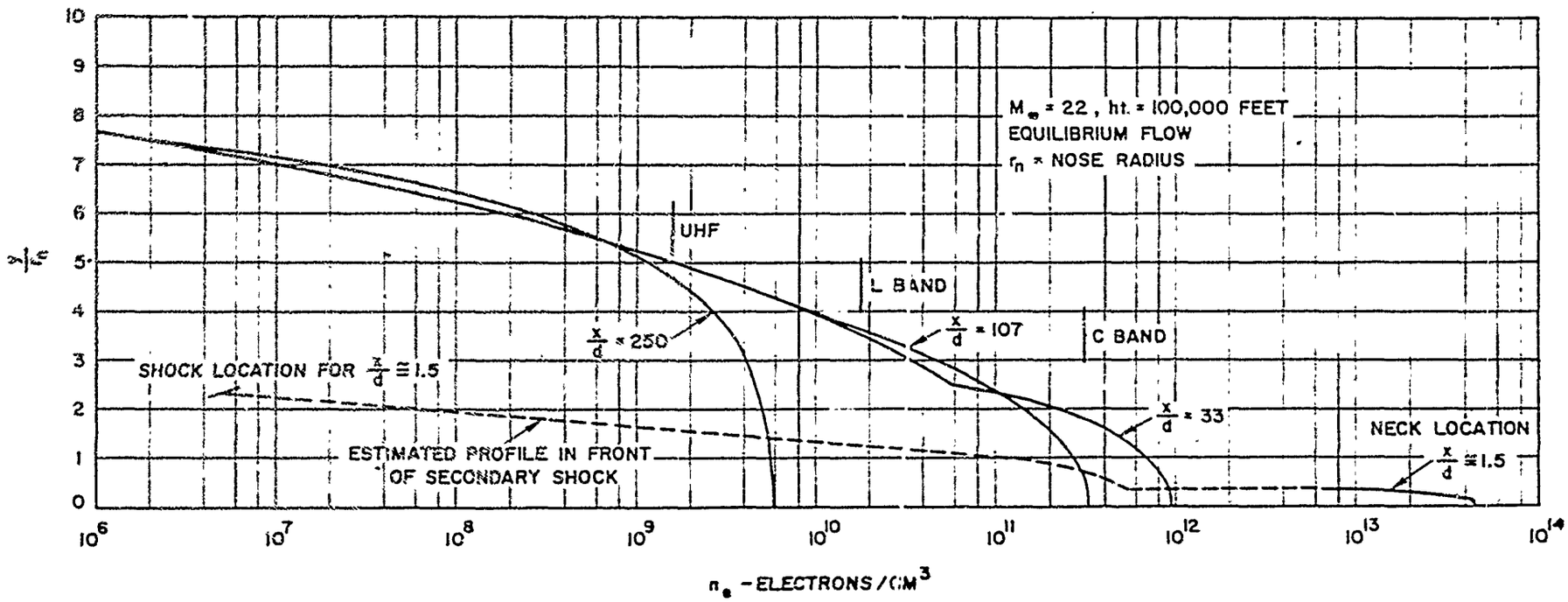
M_∞ = 22 , ht. = 100,000 FEET
EQUILIBRIUM FLOW
r_n = NOSE RADIUS
UHF
L BAND
C BAND
$\frac{x}{d}$ = 250
$\frac{x}{d}$ = 107
$\frac{x}{d}$ = 33
SHOCK LOCATION FOR $\frac{x}{d} \cong 1.5$
ESTIMATED PROFILE IN FRONT OF SECONDARY SHOCK
NECK LOCATION
$\frac{x}{d} \cong 1.5$
y/r_n
n_e - ELECTRONS / CM^3

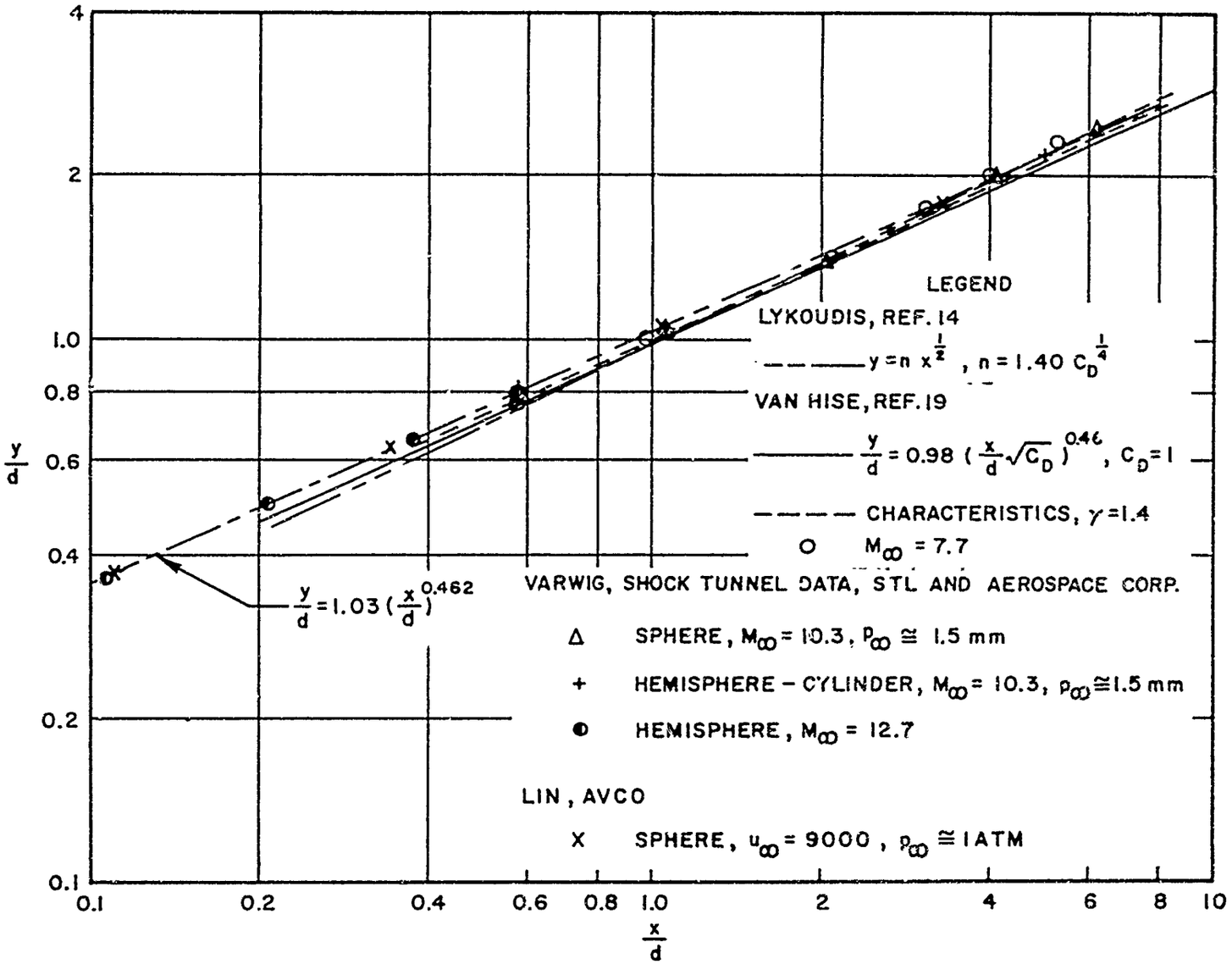

Figure 18. Correlation of Experimental Bow Shock Shapes for a Hemisphere at $M_\infty \approx 8.5$

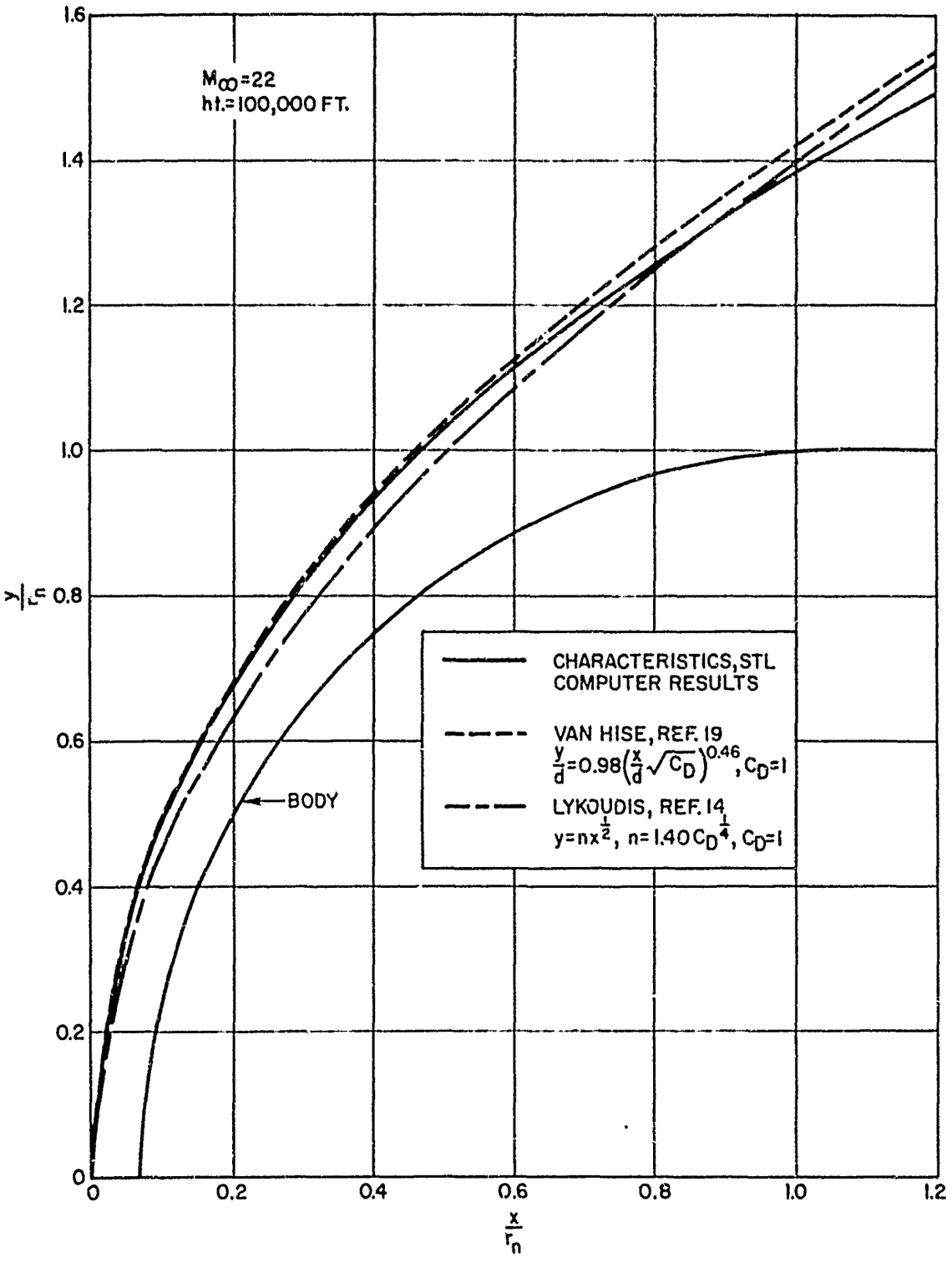

Figure 19. Bow Shock Shapes for a Hemisphere at M_∞ = 22 and 100,000 ft Altitude